

# 1 Mass balance of the Greenland Ice Sheet, 1992-2018

2 The IMBIE Team\*

## 3 Abstract

4 In recent decades the Greenland Ice Sheet has been a major contributor to global sea-level rise <sup>1,2</sup>,  
5 and it is expected to be so in the future <sup>3</sup>. Increases in glacier flow <sup>4-6</sup> and melting from the ice  
6 sheet surface <sup>7-9</sup> have been driven by oceanic <sup>10-13</sup> and atmospheric <sup>14,15</sup> warming. Here we compare  
7 and combine 26 individual satellite measurements of changes in the ice sheet's volume, flow and  
8 gravitational potential to produce a reconciled estimate of its mass balance. Although the ice  
9 sheet was close to a state of balance in the 1990's, annual losses rose steadily to peak at  $336 \pm 72$   
10 billion tonnes per year in 2012. In all, Greenland lost  $3928 \pm 341$  billion tonnes of ice between 1992  
11 and 2018, corresponding to an increase in mean sea level of  $10.8 \pm 0.9$  millimetres. Using three  
12 regional climate models, we show that reduced surface mass balance has driven  $2028 \pm 509$  billion  
13 tonnes (53 %) of the ice loss, owing to increased meltwater runoff.  $1907 \pm 547$  billion tonnes of all  
14 ice losses (47 %) are due to increased glacier discharge, which rose from  $30 \pm 34$  billion tonnes per  
15 year in the 1990's to  $88 \pm 37$  billion tonnes per year since then. Between 2013 and 2017, the total  
16 rate of ice loss slowed to  $217 \pm 19$  billion tonnes per year, on average, as atmospheric circulation  
17 favoured cooler conditions <sup>16</sup> and as ocean temperatures fell at the terminus of Jakobshavn Isbræ  
18 <sup>17</sup>. Cumulative ice losses from Greenland as a whole have been close to the IPCC's predicted rates  
19 for their high-end climate warming scenario <sup>18</sup>, which forecast an additional 70 to 130 millimetres  
20 of global sea-level rise by 2100 when compared to their central estimate.

## 21 Introduction

22 The Greenland Ice Sheet holds enough water to raise mean global sea level by 7.4 m <sup>19</sup>. Its ice flows  
23 to the oceans through a network of glaciers and ice streams <sup>20</sup>, each with a substantial inland  
24 catchment <sup>21</sup>. Fluctuations in the mass of the Greenland Ice Sheet occur due to variations in snow  
25 accumulation, meltwater runoff, ocean-driven melting, and iceberg calving. In recent decades, there  
26 have been marked increases in air <sup>22</sup> and ocean <sup>12</sup> temperatures and reductions in summer cloud  
27 cover <sup>23</sup> around Greenland. These changes have produced increases in surface runoff <sup>8,24</sup>,  
28 supraglacial lake formation <sup>25</sup> and drainage <sup>26</sup>, iceberg calving <sup>27,28</sup>, glacier terminus retreat <sup>29,30</sup>,  
29 submarine melting <sup>10,11</sup>, and ice flow <sup>4</sup>, leading to widespread changes in the ice sheet surface  
30 elevation, particularly near its margin (Figure 1).

31 Over recent decades, ice losses from Greenland have made a significant contribution to global sea-  
32 level rise <sup>2</sup>, and model projections suggest that this imbalance will continue in a warming climate <sup>3</sup>.  
33 Since the early 1990's there have been comprehensive satellite observations of changing ice sheet  
34 velocity <sup>4,5,31</sup>, elevation <sup>32-36</sup> and, between 2002 and 2016, its changing gravitational attraction <sup>37,38</sup>,  
35 from which complete estimates of Greenland Ice Sheet mass balance are determined <sup>1</sup>. Prior to the  
36 1990's, only partial surveys of the ice sheet elevation <sup>39</sup> and velocity <sup>40</sup> change are available. In  
37 combination with models of surface mass balance (the net difference between precipitation,  
38 sublimation and meltwater runoff) and glacial isostatic adjustment <sup>41</sup>, satellite measurements have  
39 shown a fivefold increase in the rate of ice loss from Greenland overall, rising from  $51 \pm 65$  Gt/yr in  
40 the early 1990's to  $263 \pm 30$  Gt/yr between 2005 and 2010 <sup>1</sup>. This ice loss has been driven by changes  
41 in surface mass balance <sup>7,22</sup> and ice dynamics <sup>6,40</sup>. There was, however, a marked reduction in ice loss  
42 between 2013 and 2018, as a consequence of cooler atmospheric conditions and increased  
43 precipitation <sup>16</sup>. While the broad pattern of change across Greenland (Figure 1) is one of ice loss,

44 there is considerable variability; for example, during the 2000's just 4 glaciers were responsible for  
45 half of the total ice loss due to increased discharge <sup>6</sup>, whereas many others contribute today <sup>40</sup>.  
46 Moreover, some neighbouring ice streams have been observed to speed up over this period while  
47 others slowed down <sup>42-44</sup>, suggesting diverse reasons for the changes that have taken place -  
48 including their geometrical configuration and basal conditions, as well as the forcing they have  
49 experienced <sup>45</sup>. In this study we combine satellite altimetry, gravimetry, and ice velocity  
50 measurements to produce a reconciled estimate of the Greenland Ice Sheet mass balance between  
51 1992 and 2018, we evaluate the impact of changes in surface mass balance and uncertainty in glacial  
52 isostatic adjustment, and we partition the ice sheet mass loss into signals associated with surface  
53 mass balance and ice dynamics. In doing so, we extend a previous assessment <sup>1</sup> to include more  
54 satellite and ancillary data and to cover the period since 2012.

## 55 Data and Methods

56 We use 26 estimates of ice sheet mass balance derived from satellite altimetry (9 data sets), satellite  
57 gravimetry (14 data sets) and the input-output method (3 data sets) to assess changes in Greenland  
58 ice sheet mass balance. The satellite data were computed using common spatial <sup>21,46</sup> and temporal  
59 domains, and using a range of models to estimate signals associated with changes in surface mass  
60 balance and glacial isostatic adjustment. Satellite altimetry provides direct measurements of  
61 changing ice sheet surface elevation recorded at orbit crossing points <sup>39</sup>, along repeated ground  
62 tracks <sup>33</sup>, or using plane-fit solutions <sup>35</sup>, and the ice sheet mass balance is estimated from these  
63 measurements either by prescribing the density of the elevation fluctuation <sup>47</sup> or by making an  
64 explicit model-based correction for changes in firn height <sup>48</sup>. Satellite gravimetry measures  
65 fluctuations in the Earth's gravitational field as computed using either global spherical harmonic  
66 solutions <sup>37</sup> or using spatially-discrete mass concentration units <sup>38</sup>. Ice sheet mass changes are  
67 determined after making model-based corrections for glacial isostatic adjustment <sup>37</sup>. The input-  
68 output method uses model estimates of surface mass balance <sup>7</sup>, which comprises the input, and  
69 satellite observations of ice sheet velocity computed from radar <sup>4</sup> and optical <sup>49</sup> imagery combined  
70 with airborne measurements of ice thickness <sup>50</sup> to compute changes in marine-terminating glacier  
71 discharge into the oceans, which comprises the output. The overall mass balance is the difference  
72 between input and output. Not all annual surveys of ice sheet discharge are complete, and  
73 sometimes regional extrapolations have to be employed to account for gaps in coverage <sup>40</sup>. Because  
74 they provide important ancillary data, we also assess 6 models of glacial isostatic adjustment and 10  
75 models of surface mass balance.

76 To compare and aggregate the individual satellite data sets, we first adopt a common approach to  
77 derive linear rates of ice sheet mass balance over 36-month intervals (see Methods). We then  
78 compute error-weighted averages of all altimetry, gravimetry, and input-output group mass trends,  
79 and we combine these into a single reconciled estimate of the ice sheet mass balance using error-  
80 weighting of the group trends. Uncertainties in individual rates of mass change are estimated as the  
81 root sum square of the linear model misfit and their measurement error, uncertainties in group rates  
82 are estimated as the root mean square of the contributing time-series errors, and uncertainties in  
83 reconciled rates are estimated as their root mean square error divided by the square root of the  
84 number of independent groups. Cumulative uncertainties are computed as the root sum square of  
85 annual errors, an approach that has been employed in numerous studies <sup>1,18,40,51</sup> and assumes that  
86 annual errors are not correlated over time. To improve on this assumption, it will be necessary to  
87 consider the covariance of the systematic and random errors present within each mass balance  
88 solution (see Methods).

## 89 Inter-comparison of satellite and model results

90 The satellite gravimetry and satellite altimetry data used in our assessment are corrected for the  
91 effects of glacial isostatic adjustment, although the correction is relatively small for altimetry as it  
92 appears as a change in elevation and not mass. The most prominent and consistent local signals of  
93 glacial isostatic adjustment among the 6 models we have considered are two instances of uplift  
94 peaking at about 5-6 mm/yr, one centered over northwest Greenland and Ellesmere Island, and one  
95 over northeast Greenland (see Methods and Extended Data Figure 3). Although some models  
96 identify a 2 mm/yr subsidence under large parts of the central and southern parts of the ice sheet, it  
97 is absent or of lower magnitude in others, which suggests it is less certain (Extended Data Table 1).  
98 The greatest difference among model solutions is at Kangerlussuaq Glacier in the southeast where a  
99 study<sup>52</sup> has shown that models and observations agree if a localized weak Earth structure associated  
100 with overpassing the Iceland hotspot is assumed; the effect is to offset earlier estimates of mass  
101 trends associated with glacial isostatic adjustment by about 20 Gt/yr. Farther afield, the highest  
102 spread between modelled uplift occurs on Baffin Island and beyond due to variations in regional  
103 model predictions related to the demise of the Laurentide Ice Sheet<sup>52,53</sup>. This regional uncertainty is  
104 likely a major factor in the spread across the ice-sheet-wide estimates. Nevertheless, at  $-3 \pm 20$   
105 Gt/yr, the mass signal associated with glacial isostatic adjustment in Greenland shows no coherent  
106 substantive change and is negligible relative to reported ice sheet mass trends<sup>1</sup>.

107 There is generally good agreement between the models of Greenland Ice Sheet surface mass  
108 balance that we have assessed for determining mass input - particularly those of a similar class; for  
109 example, 70% of all model estimated of runoff and accumulation fall within 1-sigma of their mean  
110 (see Methods and Extended Data Table 2). The exceptions are a global reanalysis with coarse spatial  
111 resolution that tends to underestimate runoff due to its poor delineation of the ablation zone, and a  
112 snow process model that tends to underestimate precipitation and to overestimate runoff in most  
113 sectors. Among the other 8 models, the average surface mass balance between 1980 and 2012 is  
114  $361 \pm 40$  Gt/yr, with a marked negative trend over time (Extended Data Figure 4) mainly due to  
115 increased runoff<sup>7</sup>. At regional scale, the largest differences occur in the northeast, where two  
116 regional climate models predict significantly less runoff, and in the southeast, where there is  
117 considerable spread in precipitation and runoff across all models. All models show high temporal  
118 variability in surface mass balance components, and all models show that the southeast receives the  
119 highest net intake of mass at the surface due to high rates of snowfall originating from the Icelandic  
120 Low<sup>54</sup>. By contrast, the southwest, which features the widest ablation zone<sup>7</sup>, has experienced  
121 alternate periods of net surface mass loss and gain over recent decades, and has the lowest average  
122 surface mass balance across the ice sheet.

123 We assessed the consistency of the satellite altimetry, gravimetry, and input-output method  
124 estimates of Greenland Ice Sheet mass balance using common spatial and temporal domains (see  
125 Figure 2 and Methods). In general, there is close agreement between estimates determined using  
126 each approach, and the standard deviations of coincident altimetry, gravimetry, and input-output  
127 method annual mass balance solutions are 31, 26, and 22 Gt/yr, respectively (Extended Data Table  
128 3). Once averages were formed for each technique, the resulting estimates of mass balance were  
129 also closely aligned (e.g. Extended Data Figure 6). For example, over the common period 2005 to  
130 2015, the average Greenland Ice Sheet mass balance is  $-249 \pm 61$  Gt/yr and, by comparison, the  
131 spread of the altimetry, gravimetry, and input-output method estimates is just 36 Gt/yr (Extended  
132 Data Table 3). The estimated uncertainty of the aggregated mass balance solution (see Methods) is  
133 larger than the standard deviation of model corrections for glacial isostatic adjustment (20 Gt/yr for  
134 gravimetry) and for surface mass balance (40 Gt/yr), which suggests that their collective impacts

135 have been adequately compensated, and it is also larger than the estimated 30 Gt/yr mass losses  
136 from peripheral ice caps<sup>55,56</sup>, which are not accounted for in all individual solutions. In keeping with  
137 results from Antarctica<sup>51</sup>, rates of mass loss determined using the input-output method are the  
138 most negative, and those determined from altimetry are the least negative. However, the spread  
139 among the three techniques is 5 times lower for Greenland than it is for Antarctica<sup>51</sup>, reflecting  
140 differences in the ice sheet size, the complexity of the mass balance processes, and limitations of the  
141 various geodetic techniques.

## 142 Ice sheet mass balance

143 We aggregated the average mass balance estimates from gravimetry, altimetry and the input-output  
144 method to form a single, time-varying record (Figure 2) and then integrated these data to determine  
145 the cumulative mass lost from Greenland since 1992 (Figure 3). Although Greenland has been losing  
146 ice throughout most of the intervening period, the rate of loss has varied significantly. Between 1992  
147 and 2012, the rate of ice loss progressively increased, reaching a maximum of **336 ± 72** Gt/yr in  
148 2012, coinciding with the extreme summertime surface melting that occurred in that year<sup>57</sup>. Since  
149 2012, however, the trend has reversed, with a progressive reduction in the rate of mass loss during  
150 the subsequent period. By 2018 – the last complete year of our survey – the annual rate of ice mass  
151 loss had reduced to **144 ± 57** Gt/yr. The highly variable nature of ice losses from Greenland is a  
152 consequence of the wide range of physical processes that are affecting different sectors of the ice  
153 sheet<sup>17,35,44</sup>, which suggests that care should be taken when extrapolating sparse measurements in  
154 space or time. Although the rates of mass loss we have computed between 1992 and 2011 are 18 %  
155 less negative than those of a previous assessment, which included far fewer data sets<sup>1</sup>, the results  
156 are consistent given their respective uncertainties. Altogether, the Greenland Ice Sheet has lost **3928**  
157 **± 341** Gt of ice to the ocean since 1992, with roughly half of this loss occurring during the 6-year  
158 period between 2006 and 2012.

159 To determine the proportion of mass lost due to surface and ice dynamical processes, we computed  
160 the contemporaneous trend in Greenland Ice Sheet surface mass balance - the net balance between  
161 precipitation and ablation<sup>7</sup>, which is controlled by interactions with the atmosphere (Figure 3). In  
162 Greenland, recent trends in surface mass balance have been largely driven by meltwater runoff<sup>54</sup>,  
163 which has increased as the regional climate has warmed<sup>14</sup>. Because direct observations of ice sheet  
164 surface mass balance are too scarce to provide full temporal and spatial coverage<sup>58</sup>, regional  
165 estimates are usually taken from atmospheric models that are evaluated with existing observations.  
166 Our evaluation (see Methods) shows that the finer spatial resolution regional climate models  
167 produce consistent results, likely due to their ability to capture local changes in melting and  
168 precipitation associated with atmospheric forcing, and to resolve the full extent of the ablation zone  
169<sup>59</sup>. We therefore compare and combine estimates of Greenland surface mass balance derived from  
170 three regional climate models; RACMO2.3p2<sup>59</sup>, MARv3.6<sup>22</sup> and HIRHAM<sup>9</sup>. To assess the surface  
171 mass change across the Greenland Ice Sheet between 1980 and 2018, we accumulate surface mass  
172 balance anomalies from each of the regional climate models (Extended Data Figure 7) and average  
173 them into a single estimate (Figure 3). Surface mass balance anomalies are computed with respect  
174 to the average between 1980 and 1990, which corresponds to a period of approximate balance<sup>8</sup> and  
175 is common to all models. In this comparison, all three models show that the Greenland Ice Sheet  
176 entered abruptly into a period of anomalously low surface mass balance in the late 1990's and,  
177 when combined, they show that the ice sheet lost **2028 ± 509** Gt of its mass due to meteorological  
178 processes between 1992 and 2018 (Table 1).

179 Just over half (53 %) of all mass losses from Greenland – and much of their short-term variability –  
180 have been due to variations in the ice sheet’s surface mass balance and its indirect impacts on firn  
181 processes. For example, between 2007 and 2012, 72 % of the total ice loss ( $193 \pm 30$  Gt/yr ) was due  
182 to surface mass balance, compared to 36 % ( $87 \pm 44$  Gt/yr) over the preceding 15 years and 58 %  
183 ( $139 \pm 25$  Gt/yr) since then (Table 1). The rise in the total rate of ice loss during the late-2000s  
184 coincided with warmer atmospheric conditions, which promoted several episodes of widespread  
185 melting and runoff<sup>15,60</sup>. The reduction in surface mass loss since then is associated with a shift of the  
186 North Atlantic Oscillation, which brought about cooler atmospheric conditions and increased  
187 precipitation along the southeastern coast<sup>16</sup>. Trends in the total ice sheet mass balance are not,  
188 however, entirely due to surface mass balance and, by differencing these two signals, we can  
189 estimate the total change in mass loss due to ice dynamical imbalance – i.e. the integrated, net mass  
190 loss from those glaciers whose velocity does not equal their long-term mean (Figure 3). Although  
191 this approach is indirect, it makes use of all the satellite observations and regional climate models  
192 included in our study, overcoming limitations in the spatial and temporal sampling of ice discharge  
193 estimates derived from ice velocity and thickness data. Our estimate shows that, between 1992 and  
194 2018, Greenland lost  $1907 \pm 547$  Gt of ice due to the dynamical imbalance of glaciers relative to  
195 their steady state, accounting for 47 % of the total imbalance (Table 1). Losses due to increased ice  
196 discharge rose sharply in the early 2000’s when Jakobshavn Isbræ<sup>61-63</sup> and several other outlet  
197 glaciers in the southeast<sup>64-66</sup> sped up, and the discharge losses are now four times higher than in the  
198 1990’s. For a period between 2002 and 2007, ice dynamical imbalance was the major source of ice  
199 loss from the ice sheet as a whole, although the situation has since returned to be dominated by  
200 surface mass losses as several glaciers have slowed down<sup>17,30</sup>.

201 Despite a reduction in the overall rate of ice loss from Greenland between 2013 and 2018 (Figure 2),  
202 the ice sheet mass balance remained negative, adding  $10.8 \pm 0.9$  mm to global sea level since 1992.  
203 Although the average sea level contribution is  $0.42 \pm 0.08$  mm/yr, the five-year average rate varied  
204 by a factor 5 over the 25-year period, peaking at  $0.75 \pm 0.05$  mm/yr between 2007 and 2012. The  
205 variability in Greenland ice loss illustrates the importance of accounting for yearly fluctuations when  
206 attempting to close the global sea level budget<sup>2,67</sup>. Satellite records of ice sheet mass balance are  
207 also an important tool for evaluating numerical models of ice sheet evolution<sup>68</sup>. In their 2013  
208 assessment, the Intergovernmental Panel on Climate Change (IPCC) predicted ice losses from  
209 Greenland due to surface mass balance and glacier dynamics under a range of scenarios, beginning  
210 in 2007<sup>18</sup> (Figure 4). Although ice losses from Greenland have fluctuated considerably during the 12-  
211 year period of overlap between the IPCC predictions and our reconciled time series, the total change  
212 and average rate ( $0.70$  mm/yr) are close to the upper range predictions (0.74 mm/yr), which implies  
213 a 70 to 130 mm of sea-level rise by the year 2100 above central estimates. The drop in ice losses  
214 between 2013 and 2018, however, shifted rates towards the lower end projections, and a longer  
215 period of comparison is required to establish whether the upper trajectory will continue to be  
216 followed. Even greater sea level contribution cannot be ruled out if feedbacks between the ice sheet  
217 and other elements of the climate system are underestimated by current ice sheet models<sup>3</sup>.  
218 Although the volume of ice stored in Greenland is a small fraction of that in Antarctica (12 %), its  
219 recent losses have been  $\sim 38$  % higher<sup>51</sup> as a consequence of the relatively strong atmospheric<sup>14,15</sup>  
220 and oceanic<sup>10,11</sup> warming that has occurred in its vicinity, and its status as a major source of sea-  
221 level rise is expected to continue<sup>3,18</sup>.

## 222 Conclusions

223 We combine 26 satellite estimates of ice sheet mass balance and assess 10 models of ice sheet  
224 surface mass balance and 6 models of glacial isostatic adjustment, to show that the Greenland Ice

225 Sheet lost  $3928 \pm 341$  Gt of ice between 1992 and 2018. During the common period 2005 to 2015,  
226 the spread of mass balance estimates derived from satellite altimetry, gravimetry, and the input-  
227 output method is  $32$  Gt/yr, or  $13\%$  of the estimated rate of imbalance. The rate of ice loss has  
228 generally increased over time, rising from  $20 \pm 24$  Gt/yr between 1992 to 1997, peaking at  $269 \pm 17$   
229 Gt/yr between 2007 and 2012, and reducing to  $238 \pm 20$  Gt/yr between 2012 and 2017. Just over  
230 half ( $2028 \pm 509$  Gt, or  $53\%$ ) of the ice losses are due to reduced surface mass balance (mostly  
231 meltwater runoff) associated with changing atmospheric conditions<sup>14,15,69</sup>, and these changes have  
232 also driven the shorter-term temporal variability in ice sheet mass balance. Despite variations in the  
233 imbalance of individual glaciers<sup>5,6,40</sup>, ice losses due to increasing discharge from the ice sheet as a  
234 whole have risen steadily from  $26 \pm 35$  Gt/yr in the 1990's to  $88 \pm 37$  Gt/yr since then, and account  
235 for just under half of all losses (47 %) over the survey period.

236 Our assessment shows that estimates of Greenland Ice Sheet mass balance derived from satellite  
237 altimetry, gravimetry, and the input-output method agree to within 20 Gt/yr, that model estimates  
238 of surface mass balance agree to within 40 Gt/yr, and that model estimates of glacial isostatic  
239 adjustment agree to within 20 Gt/yr. These differences represent a small fraction ( $13\%$ ) of the  
240 Greenland Ice Sheet mass imbalance and are comparable to its estimated uncertainty ( $28$  Gt/yr).  
241 Nevertheless, there is still departure among models of glacial isostatic adjustment in northern  
242 Greenland. Spatial resolution is a key factor in the degree to which models of surface mass balance  
243 can represent ablation and precipitation at local scales, and estimates of ice sheet mass balance  
244 determined from satellite altimetry and the input-output method continue to be positively and  
245 negatively biased, respectively, compared to those based on satellite gravimetry (albeit by small  
246 amounts). More satellite estimates of ice sheet mass balance at the start (1990's) and end (2010's)  
247 of our record would help to reduce the dependence on fewer data during those periods; although  
248 new missions<sup>70,71</sup> will no doubt address the latter, further analysis of historical satellite data is  
249 required to address the former.

## 250 Acknowledgements

251 This work is an outcome of the Ice Sheet Mass Balance Inter-Comparison Exercise (IMBIE) supported  
252 by the ESA Climate Change Initiative and the NASA Cryosphere Program. A.S. was additionally  
253 supported by a Royal Society Wolfson Research Merit Award.

## 254 Author Contributions

255 A.S. and E.I. designed and led the study. E.R., B.S., M.v.d.B., I.V. and P.W. led the input–output-  
256 method, altimetry, surface mass balance (SMB), gravimetry and glacial isostatic adjustment (GIA)  
257 experiments, respectively. A.S., E.I., K.B., M.E., A.H., I.J., G.K., S.N., T.P., E.R., T.Sc., N.S., B.S., M.v.d.B.,  
258 I.V., T.W., and P.W. supervised the assessment exercise. G.M., M.E.P., and T.Sl. performed the mass  
259 balance data collation and analysis. T.Sl. performed the AR5 data analysis. P.W. and I.S. performed  
260 the GIA data analysis. M.v.W. and T.Sl. performed the SMB data analysis. A.S., E.I., K.B., M.E., N.G.,  
261 A.H., H.K., M.M., I.O., I.S., T.Sl., M.v.W., and P.W. wrote the manuscript. A.S., K.B., H.K., G.M., M.E.P.,  
262 I.S., S.B.S., T.Sl., P.W., and M.v.W. prepared the figures and tables. All authors participated in the  
263 data interpretation and commented on the manuscript.

## 264 Competing Interests

265 The authors declare no competing interests.

266 The IMBIE Team

267 Andrew Shepherd<sup>1\*</sup>, Erik Ivins<sup>2</sup>, Eric Rignot<sup>2,3</sup>, Ben Smith<sup>4</sup>, Michiel van den Broeke<sup>5</sup>, Isabella  
268 Velicogna<sup>2,3</sup>, Pippa Whitehouse<sup>6</sup>, Kate Briggs<sup>1</sup>, Ian Joughin<sup>4</sup>, Gerhard Krinner<sup>7</sup>, Sophie Nowicki<sup>8</sup>, Tony  
269 Payne<sup>9</sup>, Ted Scambos<sup>10</sup>, Nicole Schlegel<sup>2</sup>, Geruo A<sup>3</sup>, Cécile Agosta<sup>11</sup>, Andreas Ahlstrøm<sup>12</sup>, Greg  
270 Babonis<sup>13</sup>, Valentina R. Barletta<sup>14</sup>, Anders A. Bjørk<sup>15</sup>, Alejandro Blazquez<sup>16</sup>, Jennifer Bonin<sup>17</sup>, William  
271 Colgan<sup>12</sup>, Beata Csatho<sup>13</sup>, Richard Cullather<sup>18</sup>, Marcus Engdahl<sup>19</sup>, Denis Felikson<sup>8</sup>, Xavier Fettweis<sup>11</sup>,  
272 Rene Forsberg<sup>14</sup>, Anna E. Hogg<sup>1</sup>, Hubert Gallee<sup>7</sup>, Alex Gardner<sup>2</sup>, Lin Gilbert<sup>20</sup>, Noel Gourmelen<sup>21</sup>,  
273 Andreas Groh<sup>22</sup>, Brian Gunter<sup>23</sup>, Edward Hanna<sup>24</sup>, Christopher Harig<sup>25</sup>, Veit Helm<sup>26</sup>, Alexander  
274 Horvath<sup>27</sup>, Martin Horvath<sup>22</sup>, Shfaqat Khan<sup>14</sup>, Kristian K. Kjeldsen<sup>12,28</sup>, Hannes Konrad<sup>29</sup>, Peter L.  
275 Langen<sup>30</sup>, Benoit Lecavalier<sup>31</sup>, Bryant Loomis<sup>8</sup>, Scott Luthcke<sup>8</sup>, Malcolm McMillan<sup>32</sup>, Daniele Melini<sup>33</sup>,  
276 Sebastian Mernild<sup>34,35,36,37</sup>, Yara Mohajerani<sup>3</sup>, Philip Moore<sup>38</sup>, Ruth Mottram<sup>30</sup>, Jeremie Mouginot<sup>3,7</sup>,  
277 Gorka Moyano<sup>39</sup>, Alan Muir<sup>20</sup>, Thomas Nagler<sup>40</sup>, Grace Nield<sup>6</sup>, Johan Nilsson<sup>2</sup>, Brice Noël<sup>5</sup>, Ines  
278 Ootosaka<sup>1</sup>, Mark E. Pattle<sup>39</sup>, W. Richard Peltier<sup>41</sup>, Nadège Pie<sup>42</sup>, Roelof Rietbroek<sup>43</sup>, Helmut Rott<sup>40</sup>,  
279 Louise Sandberg Sørensen<sup>14</sup>, Ingo Sasgen<sup>26</sup>, Himanshu Save<sup>42</sup>, Bernd Scheuchl<sup>3</sup>, Ernst Schrama<sup>44</sup>,  
280 Ludwig Schröder<sup>22,26</sup>, Ki-Weon Seo<sup>45</sup>, Sebastian B. Simonsen<sup>14</sup>, Thomas Slater<sup>1</sup>, Giorgio Spada<sup>46</sup>, Tyler  
281 Sutterley<sup>3</sup>, Matthieu Talpe<sup>2</sup>, Lev Tarasov<sup>31</sup>, Willem Jan van de Berg<sup>5</sup>, Wouter van der Wal<sup>47</sup>, Melchior  
282 van Wessem<sup>5</sup>, Bramha Dutt Vishwakarma<sup>48</sup>, David Wiese<sup>2</sup>, David Wilton<sup>49</sup>, Thomas Wagner<sup>50</sup>, Bert  
283 Wouters<sup>5,47</sup> & Jan Wuite<sup>40</sup>

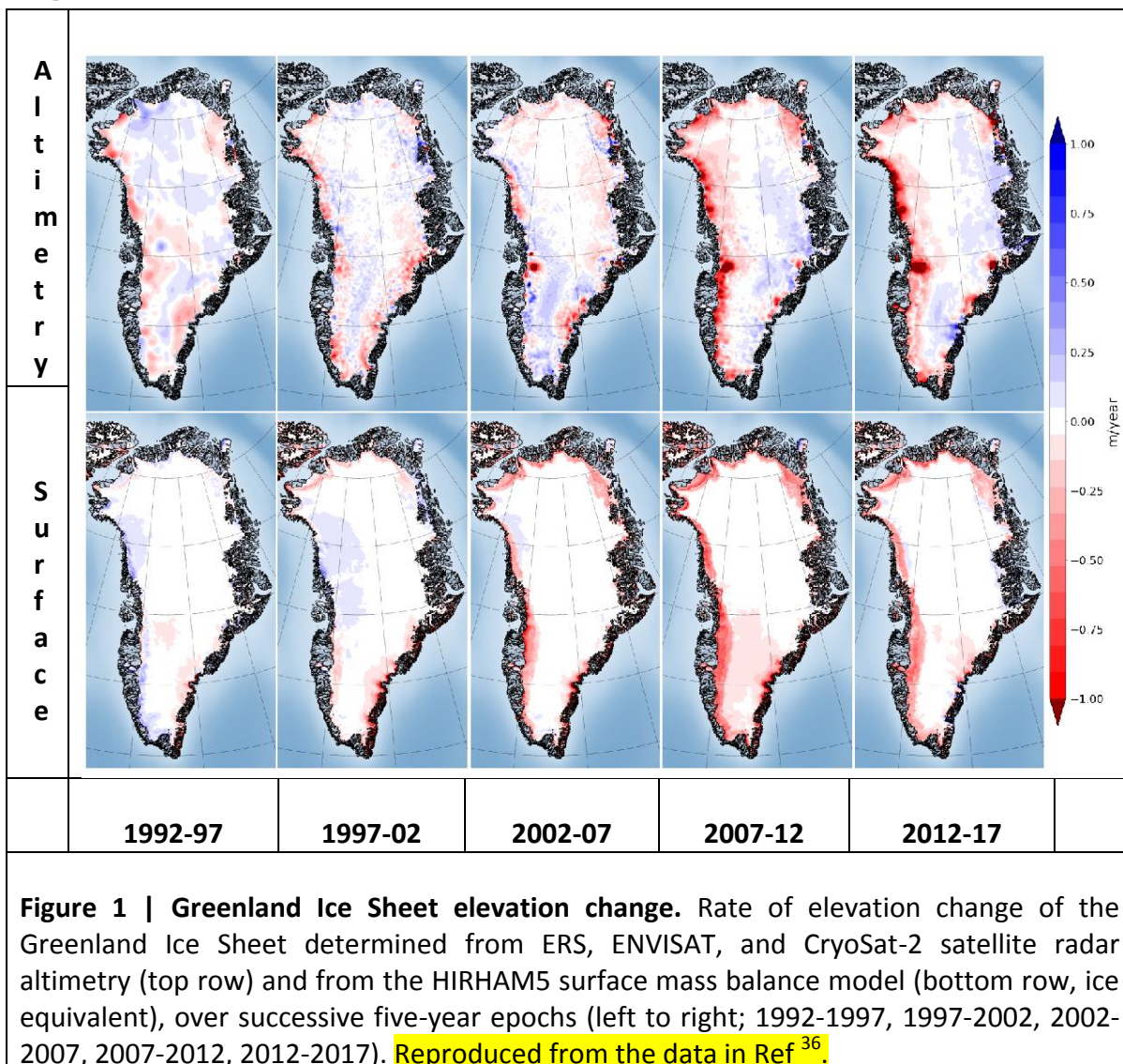
284

285 <sup>1</sup>Centre for Polar Observation and Modelling, University of Leeds, Leeds, UK. <sup>2</sup>NASA Jet Propulsion  
286 Laboratory, California Institute of Technology, Pasadena, CA, USA. <sup>3</sup>Department of Earth System  
287 Science, University of California, Irvine, CA, USA. <sup>4</sup>Department of Earth and Space Sciences,  
288 University of Washington, Seattle, WA, USA. <sup>5</sup>Institute for Marine and Atmospheric Research,  
289 Utrecht University, Utrecht, The Netherlands. <sup>6</sup>Department of Geography, Durham University,  
290 Durham, UK. <sup>7</sup>Institute of Environmental Geosciences, Université Grenoble Alpes, Grenoble, France.  
291 <sup>8</sup>Cryospheric Sciences Laboratory, NASA Goddard Space Flight Center, Greenbelt, MD, USA. <sup>9</sup>School  
292 of Geographical Sciences, University of Bristol, Bristol, UK. <sup>10</sup>Earth Science and Observation Center,  
293 University of Colorado, Boulder, CO, USA. <sup>11</sup>Department of Geography, University of Liège, Liège,  
294 Belgium. <sup>12</sup>Geological Survey of Denmark and Greenland, Copenhagen, Denmark. <sup>13</sup>Department of  
295 Geology, State University of New York at Buffalo, Buffalo, NY, USA. <sup>14</sup>DTU Space, National Space  
296 Institute, Technical University of Denmark, Kongens Lyngby, Denmark. <sup>15</sup>Department of Geosciences  
297 and Natural Resource Management, University of Copenhagen, Copenhagen, Denmark. <sup>16</sup>LEGOS,  
298 Université de Toulouse, Toulouse, France. <sup>17</sup>College of Marine Sciences, University of South Florida,  
299 Tampa, FL, USA. <sup>18</sup>Global Modeling and Assimilation Office, NASA Goddard Space Flight Center,  
300 Greenbelt, MD, USA. <sup>19</sup>ESA-ESRIN, Frascati, Italy. <sup>20</sup>Mullard Space Science Laboratory, University  
301 College London, Holmbury St Mary, UK. <sup>21</sup>School of Geosciences, University of Edinburgh, Edinburgh,  
302 UK. <sup>22</sup>Institute for Planetary Geodesy, Technische Universität Dresden, Dresden, Germany. <sup>23</sup>Daniel  
303 Guggenheim School of Aerospace Engineering, Georgia Institute of Technology, Atlanta, GA, USA.  
304 <sup>24</sup>School of Geography, University of Lincoln, Lincoln, UK. <sup>25</sup>Department of Geosciences, University of  
305 Arizona, Tucson, AZ, USA. <sup>26</sup>Alfred Wegener Institute, Helmholtz Centre for Polar and Marine  
306 Research, Bremerhaven, Germany. <sup>27</sup>Institute of Astronomical and Physical Geodesy, Technical  
307 University Munich, Munich, Germany. <sup>28</sup>GeoGenetics, Globe Institute, University of Copenhagen,  
308 Copenhagen, Denmark. <sup>29</sup>Deutscher Wetterdienst, Offenbach, Germany. <sup>30</sup>Danish Meteorological  
309 Institute, Copenhagen, Denmark. <sup>31</sup>Department of Physics and Physical Oceanography, Memorial  
310 University of Newfoundland, St. Johns, Newfoundland and Labrador, Canada. <sup>32</sup>University of  
311 Lancaster, Lancaster, UK. <sup>33</sup>Istituto Nazionale di Geofisica e Vulcanologia, Roma, Italy <sup>34</sup>Nansen  
312 Environmental and Remote Sensing Centre, Bergen, Norway. <sup>35</sup>Faculty of Engineering and Science,  
313 Western Norway University of Applied Sciences, Sogndal, Norway. <sup>36</sup>Direction of Antarctic and Sub-  
314 Antarctic Programs, Universidad de Magallanes, Punta Arenas, Chile, <sup>37</sup>Geophysical Institute,  
315 University of Bergen, Norway. <sup>38</sup>School of Engineering, Newcastle University, Newcastle upon Tyne,

316 UK. <sup>39</sup>isardSAT, Barcelona, Spain. <sup>40</sup>ENVEO, Innsbruck, Austria. <sup>41</sup>Department of Physics, University of  
317 Toronto, Toronto, Ontario, Canada. <sup>42</sup>Center for Space Research, University of Texas, Austin, TX, USA.  
318 <sup>43</sup>Institute of Geodesy and Geoinformation, University of Bonn, Bonn, Germany. <sup>44</sup>Department of  
319 Space Engineering, Delft University of Technology, Delft, The Netherlands. <sup>45</sup>Department of Earth  
320 Science Education, Seoul National University, Seoul, South Korea. <sup>46</sup>Dipartimento di Scienze Pure e  
321 Applicate, Università di Urbino "Carlo Bo", Italy. <sup>47</sup>Department of Civil Engineering, Delft University of  
322 Technology, Delft, The Netherlands. <sup>48</sup>Geodetic Institute, University of Stuttgart, Stuttgart, Germany.  
323 <sup>49</sup>Department of Computer Science, University of Sheffield, UK. <sup>50</sup>NASA Headquarters, Washington  
324 D.C., USA.

325 \*Corresponding author: Andrew Shepherd [a.shepherd@leeds.ac.uk](mailto:a.shepherd@leeds.ac.uk)

326



328

329

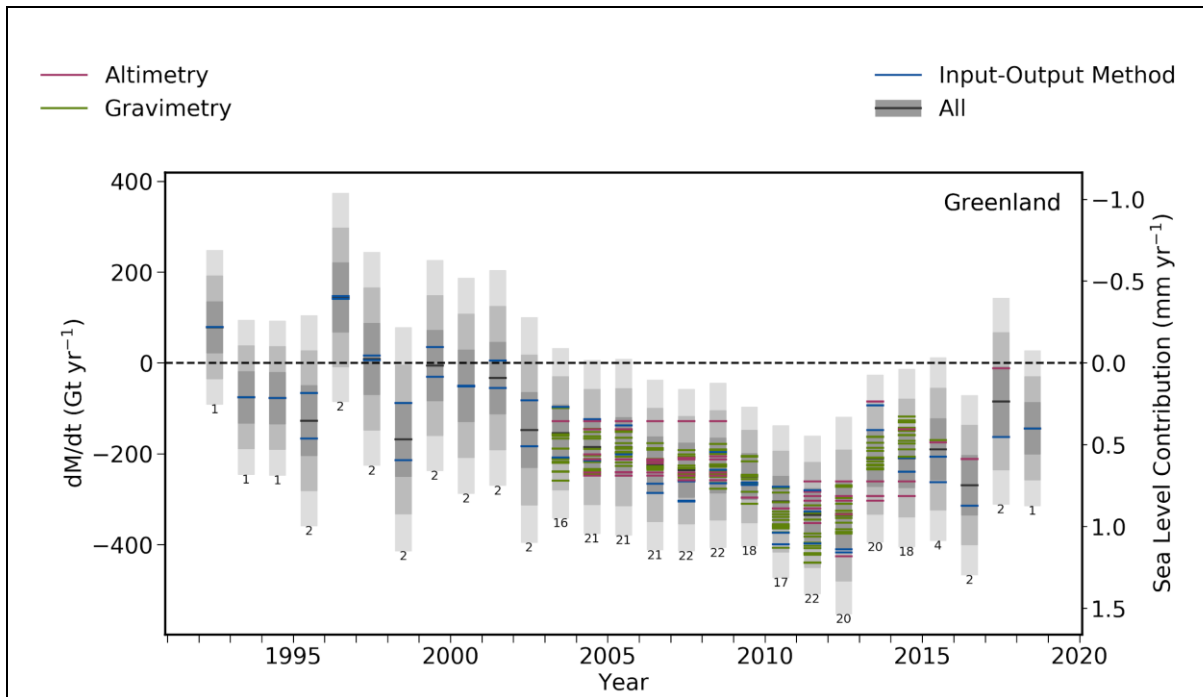


**Figure 2 | Greenland Ice Sheet mass balance.** Rate of mass change (dM/dt) of the Greenland Ice Sheet as determined from the satellite-altimetry (red), input-output method (blue) and gravimetry (green) assessments included in this study. In each case, dM/dt is computed at annual intervals from time series of relative mass change using a three-year window. An average of estimates across each class of measurement technique is also shown for each year (black). The estimated 1σ, 2σ and 3σ ranges of the class average is shaded in dark, mid and light grey, respectively; 97 % of all estimates fall within the 1σ range, given their estimated individual errors. The equivalent sea level contribution of the mass change is also indicated, and the number of individual mass-balance estimates collated at each epoch is shown below each chart entry.

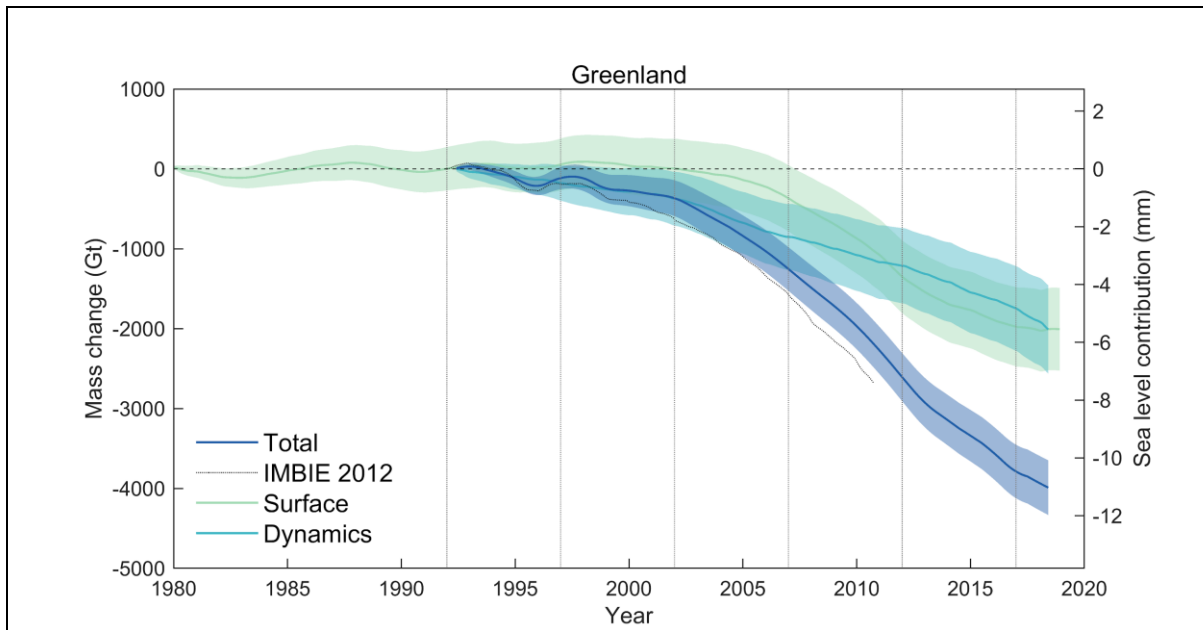


**Figure 3 | Cumulative anomalies in Greenland Ice Sheet total mass, surface mass balance and ice dynamics.** The total change (dark blue) is determined as the integral of the average rate of ice sheet mass change (Figure 2). The change in surface mass balance (green) is determined from three regional climate models relative to their mean over the period 1980-1990. The change associated with ice dynamics (light blue) is determined as the difference between the change in total and surface mass. The estimated  $1\sigma$  uncertainties of the cumulative changes are shaded. The dotted line shows the result of a previous assessment <sup>1</sup>. The equivalent sea level contribution of the mass change is also indicated. Vertical lines mark consecutive five-year epochs since the start of our satellite record in 1992.

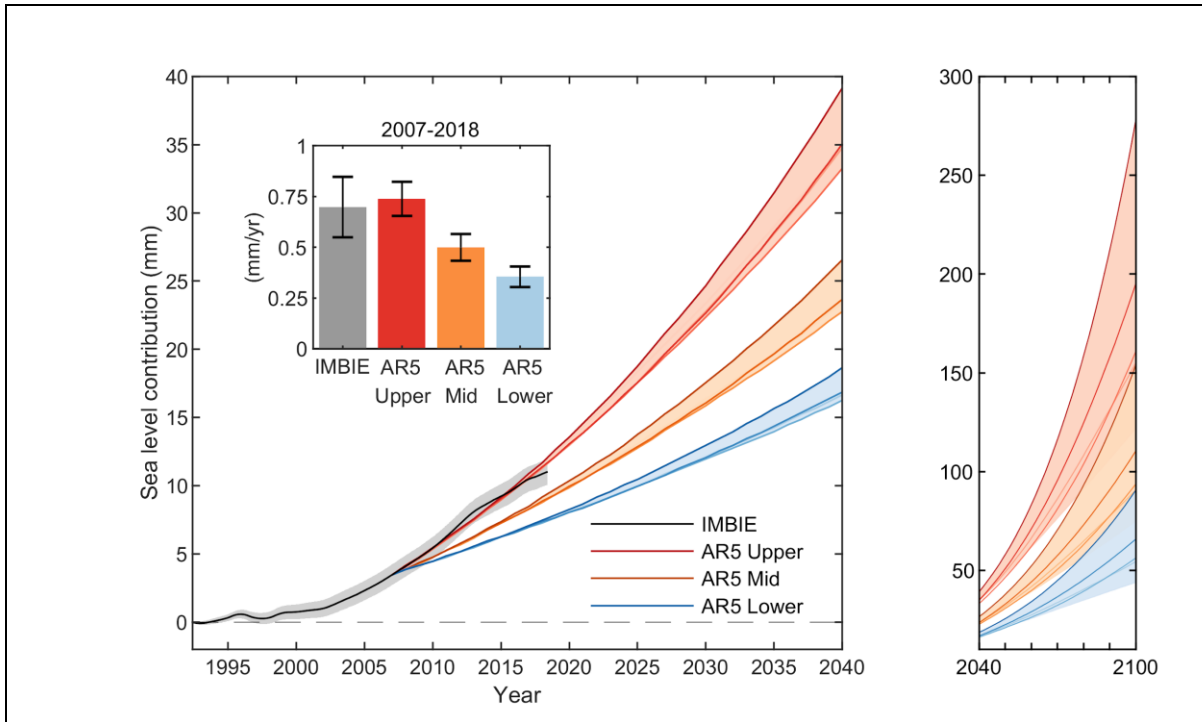


**Figure 4 | Observed and predicted sea level contribution due to Greenland Ice Sheet mass change.** The global sea-level contribution from Greenland Ice Sheet mass change according to this study (black line) and IPCC AR5 projections between 1992–2040 (left) and 2040–2100 (right) including upper (red), mid (orange), and lower (blue) estimates from the sum of modelled surface mass balance and rapid ice dynamical contributions. Darker coloured lines represent pathways from the five AR5 scenarios in order of increasing emissions: RCP2.6, RCP4.5, RCP6.0, SRES A1B and RCP8.5. Shaded areas represent the spread of AR5 emissions scenarios and the 1σ estimated error on the IMBIE data. The bar chart plot (inset) shows the average annual rates of sea-level rise (in mm/yr) during the overlap period 2007–2018 and their standard deviations. Cumulative AR5 projections have been offset to make them equal to the observational record at their start date (2007).

Region	1992-1997 (Gt/yr)	1997-2002 (Gt/yr)	2002-2007 (Gt/yr)	2007-2012 (Gt/yr)	2012-2017 (Gt/yr)	1992-2011 (Gt/yr)	1992-2018 (Gt/yr)
Total	-20 ± 24	-48 ± 25	-175 ± 20	-269 ± 17	-238 ± 20	-117 ± 24	-150 ± 28
Surface	6 ± 22	-15 ± 25	-78 ± 29	-193 ± 30	-139 ± 25	-62 ± 31	-79 ± 33
Dynamics	-26 ± 35	-33 ± 31	-97 ± 34	-76 ± 34	-100 ± 29	-55 ± 38	-70 ± 40

**Table 1 | Rates of Greenland Ice Sheet total, surface, and dynamical mass change.** Total rates were determined from all satellite measurements over various epochs, rates of surface mass change were determined from three regional climate models, and rates of dynamical mass change were determined as the difference. The period 1992–2011 is included for comparison to a previous assessment <sup>1</sup>, which reported a mass-balance estimate of -142 ± 49 Gt/yr based on far fewer data. The small differences in our updated estimate is due to our inclusion of more data and an updated aggregation

scheme (see Methods). Errors are  $1\sigma$ .

338

## 339 References

- 340 1 Shepherd, A. et al. A reconciled estimate of ice-sheet mass balance. *Science* 338, 1183-1189,  
341 doi:10.1126/science.1228102 (2012).
- 342 2 Cazenave, A. et al. Global sea-level budget 1993-present. *Earth Sys. Sci. Data* 10, 1551-1590,  
343 doi:10.5194/essd-10-1551-2018 (2018).
- 344 3 Pattyn, F. et al. The Greenland and Antarctic ice sheets under 1.5 °C global warming. *Nat.*  
345 *Clim. Change* 8, 1053-1061, doi:10.1038/s41558-018-0305-8 (2018).
- 346 4 Rignot, E. & Kanagaratnam, P. Changes in the velocity structure of the Greenland ice sheet.  
347 *Science* 311, 986-990 (2006).
- 348 5 Moon, T., Joughin, I., Smith, B. & Howat, I. 21st-century evolution of Greenland outlet glacier  
349 velocities. *Science* 336, 576-578, doi:10.1126/science.1219985 (2012).
- 350 6 Enderlin, E. M. et al. An improved mass budget for the Greenland ice sheet. *Geophysical*  
351 *Research Letters* 41, 866-872, doi:10.1002/2013GL059010 (2014).
- 352 7 Van Den Broeke, M. et al. Partitioning recent Greenland mass loss. *Science* 326, 984-986,  
353 doi:10.1126/science.1178176 (2009).
- 354 8 Trusel, L. D. et al. Nonlinear rise in Greenland runoff in response to post-industrial Arctic  
355 warming. *Nature* 564, 104-108, doi:10.1038/s41586-018-0752-4 (2018).
- 356 9 Lucas-Picher, P. et al. Very high resolution regional climate model simulations over  
357 Greenland: Identifying added value. *J. Geophys. Res. D Atmos.* 117,  
358 doi:10.1029/2011JD016267 (2012).
- 359 10 Holland, D. M., Thomas, R. H., De Young, B., Ribergaard, M. H. & Lyberth, B. Acceleration of  
360 Jakobshavn Isbrae triggered by warm subsurface ocean waters. *Nature Geoscience* 1, 659-  
361 664 (2008).
- 362 11 Seale, A., Christoffersen, P., Mugford, R. I. & O'Leary, M. Ocean forcing of the Greenland Ice  
363 Sheet: Calving fronts and patterns of retreat identified by automatic satellite monitoring of  
364 eastern outlet glaciers. *J. Geophys. Res. F Earth Surf.* 116, doi:10.1029/2010JF001847 (2011).
- 365 12 Straneo, F. & Heimbach, P. North Atlantic warming and the retreat of Greenland's outlet  
366 glaciers. *Nature* 504, 36-43, doi:10.1038/nature12854 (2013).
- 367 13 Rignot, E., Fenty, I., Menemenlis, D. & Xu, Y. Spreading of warm ocean waters around  
368 Greenland as a possible cause for glacier acceleration. *Annals of Glaciology* 53, 257-266,  
369 doi:10.3189/2012AoG60A136 (2012).
- 370 14 Hanna, E., Mernild, S. H., Cappelen, J. & Steffen, K. Recent warming in Greenland in a long-  
371 term instrumental (1881-2012) climatic context: I. Evaluation of surface air temperature  
372 records. *Environ.Res.Lett.* 7, doi:10.1088/1748-9326/7/4/045404 (2012).
- 373 15 Fettweis, X. et al. Brief communication Important role of the mid-tropospheric atmospheric  
374 circulation in the recent surface melt increase over the Greenland ice sheet. *Cryosphere* 7,  
375 241-248, doi:10.5194/tc-7-241-2013 (2013).

- 376 16 Bevis, M. et al. Accelerating changes in ice mass within Greenland, and the ice sheet's  
377 sensitivity to atmospheric forcing. *Proceedings of the National Academy of Sciences of the*  
378 *United States of America* 116, 1934-1939, doi:10.1073/pnas.1806562116 (2019).
- 379 17 Khazendar, A. et al. Interruption of two decades of Jakobshavn Isbrae acceleration and  
380 thinning as regional ocean cools. *Nature Geoscience* 12, 277-283, doi:10.1038/s41561-019-  
381 0329-3 (2019).
- 382 18 Church, J. A. et al. in *Climate Change 2013: The Physical Science Basis. Contribution of*  
383 *Working Group I to the Fifth Assessment Report of the Intergovernmental Panel on Climate*  
384 *Change* (eds T. F. Stocker et al.) Ch. 13, 1137–1216 (Cambridge University Press, 2013).
- 385 19 Morlighem, M. et al. BedMachine v3: Complete Bed Topography and Ocean Bathymetry  
386 Mapping of Greenland From Multibeam Echo Sounding Combined With Mass Conservation.  
387 *Geophysical Research Letters* 44, 11,051-011,061, doi:10.1002/2017GL074954 (2017).
- 388 20 Joughin, I., Smith, B. E., Howat, I. M., Scambos, T. & Moon, T. Greenland flow variability from  
389 ice-sheet-wide velocity mapping. *Journal of Glaciology* 56, 415-430,  
390 doi:10.3189/002214310792447734 (2010).
- 391 21 Zwally, H. J., Giovinetto, M. B., Beckley, M. A. & Saba, J. L. Antarctic and Greenland drainage  
392 systems. GSFC Cryospheric Sciences Laboratory.  
393 [https://icesat4.gsfc.nasa.gov/cryo\\_data/ant\\_grn\\_drainage\\_systems.php](https://icesat4.gsfc.nasa.gov/cryo_data/ant_grn_drainage_systems.php) (2012).
- 394 22 Fettweis, X. et al. Reconstructions of the 1900-2015 Greenland ice sheet surface mass  
395 balance using the regional climate MAR model. *Cryosphere* 11, 1015-1033, doi:10.5194/tc-  
396 11-1015-2017 (2017).
- 397 23 Hofer, S., Tedstone, A. J., Fettweis, X. & Bamber, J. L. Decreasing cloud cover drives the  
398 recent mass loss on the Greenland Ice Sheet. *Sci. Adv.* 3, doi:10.1126/sciadv.1700584 (2017).
- 399 24 Van Den Broeke, M. R. et al. On the recent contribution of the Greenland ice sheet to sea  
400 level change. *Cryosphere* 10, 1933-1946, doi:10.5194/tc-10-1933-2016 (2016).
- 401 25 Leeson, A. A. et al. Supraglacial lakes on the Greenland ice sheet advance inland under  
402 warming climate. *Nat. Clim. Change* 5, 51-55, doi:10.1038/nclimate2463 (2015).
- 403 26 Palmer, S., McMillan, M. & Morlighem, M. Subglacial lake drainage detected beneath the  
404 Greenland ice sheet. *Nat. Commun.* 6, doi:10.1038/ncomms9408 (2015).
- 405 27 Nick, F. M. et al. The response of Petermann Glacier, Greenland, to large calving events, and  
406 its future stability in the context of atmospheric and oceanic warming. *Journal of Glaciology*  
407 58, 229-239, doi:10.3189/2012JoG11J242 (2012).
- 408 28 Amundson, J. M. et al. Glacier, fjord, and seismic response to recent large calving events,  
409 Jakobshavn Isbræ, Greenland. *Geophysical Research Letters* 35, doi:10.1029/2008GL035281  
410 (2008).
- 411 29 Joughin, I. et al. Ice-front variation and tidewater behavior on Helheim and Kangerdlugssuaq  
412 Glaciers, Greenland. *J. Geophys. Res. F Earth Surf.* 113, doi:10.1029/2007JF000837 (2008).
- 413 30 Lemos, A. et al. Ice velocity of Jakobshavn Isbræ, Petermann Glacier, Nioghalvfjærdsfjorden,  
414 and Zachariæ Isstrøm, 2015-2017, from Sentinel 1-a/b SAR imagery. *Cryosphere* 12, 2087-  
415 2097, doi:10.5194/tc-12-2087-2018 (2018).

- 416 31 Nagler, T., Rott, H., Hetzenecker, M., Wuite, J. & Potin, P. The Sentinel-1 mission: New  
417 opportunities for ice sheet observations. *Remote Sens.* 7, 9371-9389,  
418 doi:10.3390/rs70709371 (2015).
- 419 32 Krabill, W. et al. Greenland ice sheet: High-elevation balance and peripheral thinning.  
420 *Science* 289, 428-430 (2000).
- 421 33 Pritchard, H. D., Arthern, R. J., Vaughan, D. G. & Edwards, L. A. Extensive dynamic thinning  
422 on the margins of the Greenland and Antarctic ice sheets. *Nature* 461, 971-975 (2009).
- 423 34 Kjeldsen, K. K. et al. Spatial and temporal distribution of mass loss from the Greenland Ice  
424 Sheet since AD 1900. *Nature* 528, 396-400, doi:10.1038/nature16183 (2015).
- 425 35 McMillan, M. et al. A high-resolution record of Greenland mass balance. *Geophysical  
426 Research Letters* 43, 7002-7010, doi:10.1002/2016GL069666 (2016).
- 427 36 Sandberg Sørensen, L. et al. 25 years of elevation changes of the Greenland Ice Sheet from  
428 ERS, Envisat, and CryoSat-2 radar altimetry. *Earth and Planetary Science Letters* 495, 234-  
429 241, doi:10.1016/j.epsl.2018.05.015 (2018).
- 430 37 Velicogna, I. & Wahr, J. Greenland mass balance from GRACE. *Geophysical Research Letters*  
431 32, art-L18505 (2005).
- 432 38 Luthcke, S. B. et al. Recent Greenland Ice Mass Loss by Drainage System from Satellite  
433 Gravity Observations. *Science* 314, 1286-1289 (2006).
- 434 39 Zwally, H. J., Brenner, A. C., Major, J. A., Bindschadler, R. A. & Marsh, J. G. Growth of  
435 Greenland ice sheet: Measurement. *Science* 246, 1587-1589,  
436 doi:10.1126/science.246.4937.1587 (1989).
- 437 40 Mougnot, J. et al. Forty-six years of Greenland Ice Sheet mass balance from 1972 to 2018.  
438 *Proceedings of the National Academy of Sciences of the United States of America* (2019).
- 439 41 Lecavalier, B. S. et al. A model of Greenland ice sheet deglaciation constrained by  
440 observations of relative sea level and ice extent. *Quaternary Science Reviews* 102, 54-84,  
441 doi:10.1016/j.quascirev.2014.07.018 (2014).
- 442 42 Felikson, D. et al. Inland thinning on the Greenland ice sheet controlled by outlet glacier  
443 geometry. *Nature Geoscience* 10, 366-369, doi:10.1038/ngeo2934 (2017).
- 444 43 Mougnot, J., Rignot, E., Scheuchl, B. & Millan, R. Comprehensive annual ice sheet velocity  
445 mapping using Landsat-8, Sentinel-1, and RADARSAT-2 data. *Remote Sens.* 9,  
446 doi:10.3390/rs9040364 (2017).
- 447 44 King, M. D. et al. Seasonal to decadal variability in ice discharge from the Greenland Ice  
448 Sheet. *Cryosphere* 12, 3813-3825, doi:10.5194/tc-12-3813-2018 (2018).
- 449 45 Porter, D. F. et al. Identifying Spatial Variability in Greenland's Outlet Glacier Response to  
450 Ocean Heat. *Front. Earth Sci.* 6, doi:10.3389/feart.2018.00090 (2018).
- 451 46 Rignot, E. & Mougnot, J. Ice flow in Greenland for the International Polar Year 2008-2009.  
452 *Geophysical Research Letters* 39, doi:10.1029/2012GL051634 (2012).
- 453 47 Sorensen, L. S. et al. Mass balance of the Greenland ice sheet (2003-2008) from ICESat data -  
454 the impact of interpolation, sampling and firn density. *Cryosphere* 5, 173-186 (2011).

- 455 48 Zwally, H. J. et al. Greenland ice sheet mass balance: distribution of increased mass loss with  
456 climate warming; 2003-07 versus 1992-2002. *Journal of Glaciology* 57, 88-102 (2011).
- 457 49 Rosenau, R., Scheinert, M. & Dietrich, R. A processing system to monitor Greenland outlet  
458 glacier velocity variations at decadal and seasonal time scales utilizing the Landsat imagery.  
459 *Remote Sensing of Environment* 169, 1-19, doi:10.1016/j.rse.2015.07.012 (2015).
- 460 50 Gogineni, S. et al. Coherent radar ice thickness measurements over the Greenland ice sheet.  
461 *Journal of Geophysical Research* 106, 33761-33772 (2001).
- 462 51 Shepherd, A. et al. Mass balance of the Antarctic Ice Sheet from 1992 to 2017. *Nature* 558,  
463 219-222, doi:10.1038/s41586-018-0179-y (2018).
- 464 52 Khan, S. A. et al. Geodetic measurements reveal similarities between post–Last Glacial  
465 Maximum and present-day mass loss from the Greenland ice sheet. *Sci. Adv.* 2,  
466 doi:10.1126/sciadv.1600931 (2016).
- 467 53 Peltier, W. R., Argus, D. F. & Drummond, R. Space geodesy constrains ice age terminal  
468 deglaciation: The global ICE-6G-C (VM5a) model. *J. Geophys. Res. B Solid Earth* 120, 450-487,  
469 doi:10.1002/2014JB011176 (2015).
- 470 54 Ettema, J. et al. Higher surface mass balance of the Greenland ice sheet revealed by high-  
471 resolution climate modeling. *Geophysical Research Letters* 36, doi:10.1029/2009GL038110  
472 (2009).
- 473 55 Bolch, T. et al. Mass loss of Greenland's glaciers and ice caps 2003-2008 revealed from  
474 ICESat laser altimetry data. *Geophysical Research Letters* 40, 875-881, doi:10.1002/grl.50270  
475 (2013).
- 476 56 Colgan, W., Luthcke, S., Abdalati, W. & Citterio, M. Constraining grace-derived cryosphere-  
477 attributed signal to irregularly shaped ice-covered areas. *Cryosphere* 7, 1901-1914,  
478 doi:10.5194/tc-7-1901-2013 (2013).
- 479 57 Tedesco, M. et al. Evidence and analysis of 2012 Greenland records from spaceborne  
480 observations, a regional climate model and reanalysis data. *The Cryosphere* 7, 615-630,  
481 doi:10.5194/tc-7-615-2013 (2013).
- 482 58 Vernon, C. L. et al. Surface mass balance model intercomparison for the Greenland ice sheet.  
483 *The Cryosphere* 7, 599-614, doi:10.5194/tc-7-599-2013 (2013).
- 484 59 Noël, B. et al. Modelling the climate and surface mass balance of polar ice sheets using  
485 RACMO2 - Part 1: Greenland (1958-2016). *Cryosphere* 12, 811-831, doi:10.5194/tc-12-811-  
486 2018 (2018).
- 487 60 Nghiem, S. V. et al. The extreme melt across the Greenland ice sheet in 2012. *Geophysical*  
488 *Research Letters* 39, doi:10.1029/2012GL053611 (2012).
- 489 61 Joughin, I., Abdalati, W. & Fahnestock, M. Large fluctuations in speed on Greenland's  
490 Jakobshavn Isbrae glacier. *Nature* 432, 608-610 (2004).
- 491 62 Joughin, I. et al. Continued evolution of Jakobshavn Isbrae following its rapid speedup. *J.*  
492 *Geophys. Res. F Earth Surf.* 113, doi:10.1029/2008JF001023 (2008).

- 493 63 Joughin, I., Smith, B. E. & Howat, I. Greenland Ice Mapping Project: Ice flow velocity variation  
494 at sub-monthly to decadal timescales. *Cryosphere* 12, 2211-2227, doi:10.5194/tc-12-2211-  
495 2018 (2018).
- 496 64 Rignot, E. Changes in ice dynamics and mass balance of the Antarctic ice sheet. *Philosophical  
497 Transactions of the Royal Society A-Mathematical Physical and Engineering Sciences* 364,  
498 1637-1655 (2006).
- 499 65 Howat, I. M., Joughin, I., Fahnestock, M., Smith, B. E. & Scambos, T. A. Synchronous retreat  
500 and acceleration of southeast Greenland outlet glaciers 2000-06: Ice dynamics and coupling  
501 to climate. *Journal of Glaciology* 54, 646-660 (2008).
- 502 66 Luckman, A., Murray, T., de Lange, R. & Hanna, E. Rapid and synchronous ice-dynamic  
503 changes in East Greenland. *Geophysical Research Letters* 33, art-L03503 (2006).
- 504 67 Dieng, H. B., Cazenave, A., Meyssignac, B. & Ablain, M. New estimate of the current rate of  
505 sea level rise from a sea level budget approach. *Geophysical Research Letters* 44, 3744-3751,  
506 doi:10.1002/2017GL073308 (2017).
- 507 68 Shepherd, A. & Nowicki, S. Improvements in ice-sheet sea-level projections. *Nat. Clim.  
508 Change* 7, 672-674, doi:10.1038/nclimate3400 (2017).
- 509 69 Fettweis, X. et al. Estimating the Greenland ice sheet surface mass balance contribution to  
510 future sea level rise using the regional atmospheric climate model MAR. *Cryosphere* 7, 469-  
511 489, doi:10.5194/tc-7-469-2013 (2013).
- 512 70 Markus, T. et al. The Ice, Cloud, and land Elevation Satellite-2 (ICESat-2): Science  
513 requirements, concept, and implementation. *Remote Sensing of Environment* 190, 260-273,  
514 doi:10.1016/j.rse.2016.12.029 (2017).
- 515 71 Flechtner, F. et al. What Can be Expected from the GRACE-FO Laser Ranging Interferometer  
516 for Earth Science Applications? *Surveys in Geophysics* 37, 453-470, doi:10.1007/s10712-015-  
517 9338-y (2016).

## 518 [Methods](#)

### 519 [Data](#)

520 In this assessment we analyse 5 groups of data: estimates of ice sheet mass-balance determined  
521 from 3 distinct classes of satellite observations - altimetry, gravimetry and the input-output method  
522 (IOM) - and model estimates of surface mass balance (SMB) and glacial isostatic adjustment (GIA).  
523 Each dataset is computed following previously reported methods (Supplementary Table 1) and, for  
524 consistency, they are aggregated within common spatial and temporal domains. Altogether, 26  
525 separate ice sheet mass balance datasets were used - 9 derived from satellite altimetry, 3 derived  
526 from the input-output method, and 14 derived from satellite gravimetry - with a combined period  
527 running from 1992 to 2018 (Extended Data Figure 1). We also assess 6 model estimates of GIA  
528 (Extended Data Table 1) and 10 model estimates of SMB (Extended Data Table 2).

### 529 [Drainage Basins](#)

530 We analyse mass trends using two ice sheet drainage basin sets (Extended Data Figure 2), to allow  
531 consistency with those used in the first IMBIE assessment <sup>1</sup>, and to evaluate an updated definition  
532 tailored towards mass budget assessments. The first set comprises 19 drainage basins delineated  
533 using surface elevation maps derived from ICESat-1 with a total area of 1,703,625 km<sup>2</sup> <sup>21</sup>. The second

534 drainage basin set is an updated definition considering other factors such as the direction of ice flow  
535 and includes 6 basins with a combined area of 1,723,300 km<sup>2</sup> <sup>46</sup>. The two drainage basin sets differ  
536 by 1% in area at the scale of the Greenland Ice Sheet, and this has a negligible impact on mass trends  
537 when compared to the estimated uncertainty of individual techniques.

### 538 [Glacial isostatic adjustment](#)

539 GIA - the delayed response of Earth's interior to temporal changes in ice loading - affects estimates  
540 of ice sheet mass balance determined from satellite gravimetry and, to a lesser extent, satellite  
541 altimetry <sup>72</sup>. Here, we compare 6 independent models of GIA in the vicinity of the Greenland Ice  
542 Sheet (Extended Data Table 1). The GIA model solutions differ for a variety of reasons, including  
543 differences in their physics, in their computational approach, in their prescriptions of solid Earth  
544 unloading during the last glacial cycle and their Earth rheology, and in the data sets against which  
545 they are evaluated. No approach is generally accepted as optimal, and so we evaluate the models by  
546 computing the mean and standard deviation of their predicted uplift rates (Extended Data Figure 3).  
547 We also estimate the contribution of each model to gravimetric mass trends using a common  
548 processing approach <sup>51</sup> which puts special emphasis on the treatment of low spherical harmonic  
549 degrees in the GIA-related trends in the gravitational field.

550 The highest rates of GIA-related uplift occur in northern Greenland - though this region also exhibits  
551 marked variability among the solutions, as does the area around Kangerlussuaq Glacier to the  
552 southeast. Even though the model spread is high in northern Greenland, the signal in this sector is  
553 also consistently high in most solutions. However, none of the GIA models considered here fully  
554 captures all areas of high uplift present in the models, and so it is possible there is a bias towards  
555 low values in the average field across the ice sheet overall. The models yield an average adjustment  
556 for GRACE estimates of Greenland Ice Sheet mass balance of -3 Gt/yr, with a standard deviation of  
557 around 20 Gt/yr. The spread is likely in part due to differences in the way each model accounts for  
558 GIA in North America which is ongoing and impacts western Greenland, and so care must be taken  
559 when estimating mass balance at basin scale. Local misrepresentation of the solid Earth response  
560 can also have a relatively large impact stemming especially from lateral variations of solid-Earth  
561 properties <sup>52</sup>, and revisions of the current state of knowledge can be expected <sup>41</sup>.

### 562 [Surface mass balance](#)

563 Here, ice-sheet SMB is defined as total precipitation minus sublimation, evaporation and meltwater  
564 runoff, i.e. the interaction of the atmosphere and the superficial snow and firn layers, for example  
565 through mass exchanges via precipitation, sublimation, and runoff, and through mass redistribution  
566 by snowdrift, melting, and refreezing. We compare 10 estimates of Greenland Ice Sheet SMB derived  
567 using a range of alternative approaches; 4 regional climate models (RCM's), 2 downscaled RCM's, a  
568 global reanalysis, 2 downscaled model reanalyses of climate data, and 1 gridded model of snow  
569 processes driven by climate model output (Extended Data Table 2).

570 Although SMB models of similar class tend to produce similar results, there are larger differences  
571 between classes – most notably the global reanalysis and the process model which lead to estimates  
572 of SMB that are significantly higher and lower than all other solutions, respectively. The regional  
573 climate model solutions agree well at the scale of individual drainage sectors, with the largest  
574 differences occurring in north-east Greenland (Extended Data Figure 4). The snow process model  
575 tends to underestimate SMB when compared to the other solutions we have considered in various  
576 sectors of the ice sheet, at times even yielding negative SMB, while the global reanalysis tends to  
577 overestimate it.

578 Across all models, the average SMB of the Greenland Ice Sheet between 1980 to 2012 is 351 Gt/yr  
579 and the standard deviation is 98 Gt/yr. However, the spread among the 8 RCM's and downscaled  
580 reanalyses is considerably smaller; these solutions lead to an average Greenland Ice Sheet SMB of  
581 361 Gt/yr with a standard deviation of 40 Gt/yr over the same period. By comparison, the global  
582 reanalysis and process model lead to ice sheet wide estimates of SMB that are significantly larger  
583 (504 Gt/yr) and smaller (125 Gt/yr) than this range, respectively. Model resolution is an important  
584 factor when estimating SMB and its components, as respective contributions where only the spatial  
585 resolution differed yield regional differences. Additionally, the underlying model domains were  
586 identified as a source of discrepancy in the case of the Greenland Ice Sheet, as some products would  
587 allocate the ablation area outside the given mask.

### 588 Individual estimates of ice sheet mass balance

589 To standardise our comparison and aggregation of the 26 individual satellite estimates of Greenland  
590 Ice Sheet mass balance, we applied a common approach to derive rates of mass change from  
591 cumulative mass trends<sup>51</sup>. Rates of mass change were computed over 36-month intervals centred  
592 on regularly spaced (monthly) epochs within each cumulative mass trend time series, oversampling  
593 the individual time series where necessary. At each epoch, rates of mass change were estimated by  
594 fitting a linear trend to data within the surrounding 36-month time window using a weighted least-  
595 squares approach, with each point weighted by its measurement error. The associated mass trend  
596 uncertainties were estimated as the **root sum square of the regression error and the measurement**  
597 **error**. Time series were truncated by half the moving-average window period at the start and end of  
598 their period. The emerging rates of mass change were then averaged over 12-month periods to  
599 reduce the impact of seasonal cycles.

600 **Gravimetry** We include 14 estimates of Greenland Ice Sheet ice sheet mass balance determined  
601 from GRACE satellite gravimetry which together span the period 2003 to 2016 (Extended Data Figure  
602 1). 10 of the gravimetry solutions were computed using spherical harmonic solutions to the global  
603 gravity field and 4 were computed using spatially defined mass concentration units (Supplementary  
604 Table 1). **An unrestricted range** of alternative GIA corrections were used in the formation of the  
605 gravimetry mass balance solutions based on commonly-adopted model solutions and their variants  
606<sup>41,53,73-78</sup> (Supplementary Table 1). There was some variation in the sampling of the individual  
607 gravimetry data sets, and their collective effective (weighted mean) temporal resolution is 0.08  
608 years. Overall, there is good agreement between rates of Greenland Ice Sheet mass change derived  
609 from satellite gravimetry (Extended Data Figure 5); all solutions show the ice sheet to be in a state of  
610 negative mass balance throughout their survey periods, with mass loss peaking in 2012 and reducing  
611 thereafter. **During the period 2005 to 2015**, annual rates of mass change determined from satellite  
612 gravimetry differ by **86 Gt/yr on average**, and their average standard deviation is 26 Gt/yr (Extended  
613 Data Table 3).

614 **Altimetry** We include 9 estimates of Greenland Ice Sheet mass balance determined from satellite  
615 altimetry which together span the period 2004 to 2018 (Extended Data Figure 1). 3 of the solutions  
616 are derived from radar altimetry, 4 from laser altimetry, and 2 use a combination of both  
617 (Supplementary Table 1). The altimetry mass trends are also computed using a range of approaches,  
618 including crossovers, planar fits, and repeat track analyses. The laser altimetry mass trends are  
619 computed from ICESat-1 data as constant rates of mass change over their respective survey periods,  
620 while the radar altimetry mass trends are computed from EnviSat and/or CryoSat-2 data with a  
621 temporal resolution of between 1 and 72 months. In consequence, the altimetry solutions have an  
622 effective collective temporal resolution of 0.74 years. Mass changes are computed after making  
623 corrections for alternative sources of surface elevation change, including glacial isostatic and elastic

624 adjustment, and firn height changes (see Supplementary Table 1). Despite the range of input data  
625 and technical approaches, there is good overall agreement between rates of mass change  
626 determined from the various satellite altimetry solutions (Extended Data Figure 5). All altimetry  
627 solutions show the Greenland Ice Sheet to be in a state of negative mass balance throughout their  
628 survey periods, with mass loss peaking in 2012 and reducing thereafter. During the period 2005 to  
629 2015, annual rates of mass change determined from satellite altimetry differ by 84 Gt/yr on average,  
630 and, their average standard deviation is 31 Gt/yr (Extended Data Table 3). The greatest variance lies  
631 among the 4 laser altimetry mass balance solutions which range from -248 to -128 Gt/yr between  
632 2004 and 2010; aside from methodological differences, possible explanations for this high spread  
633 include the relatively short period over which the mass trends are determined, the poor temporal  
634 resolution of these data sets, and the rapid change in mass balance occurring during the period in  
635 question.

636 **Input-Output Method** We include 3 estimates of Greenland Ice Sheet mass balance determined  
637 from the input-output method which together span the period 1992 to 2015 (Extended Data Figure  
638 1). Although there are relatively few data sets by comparison to the gravimetry and altimetry  
639 solutions, the input-output data provide information on the partitioning of the mass change (surface  
640 processes and/or ice dynamics) cover a significantly longer period and are therefore an important  
641 record of changes in Greenland Ice Sheet mass during the 1990's. The input-output method makes  
642 use of a wide range of satellite imagery for computing ice sheet discharge (output), and several  
643 alternative SMB model estimates of snow accumulation (input) and runoff (output) (see  
644 Supplementary Table 1). 2 of the input-output method datasets exhibit temporal variability across  
645 their survey periods, and 2 provide only constant rates of mass changes. Although these latter  
646 records are relatively short, they are an important marker with which variances among independent  
647 estimates can be evaluated. The collective effective (weighted mean) temporal resolution of the  
648 input-output method data is 0.14 years, although it should be noted that in earlier years the satellite  
649 ice discharge component of the data are relatively sparsely sampled in time (e.g. <sup>79</sup>). There is good  
650 overall agreement between rates of mass change determined from the input-output method  
651 solutions (Extended Data Figure 5). During the period 2005 to 2015, annual rates of mass change  
652 determined from the 4 input-output data sets differ by up to 47 Gt/yr on average, and their average  
653 standard deviation is 22 Gt/yr (Extended Data Table 3). These differences are comparable to the  
654 estimated uncertainty of the individual techniques and are also small relative to the estimated mass  
655 balance over the period in question. In addition to showing that the Greenland Ice Sheet was in a  
656 state of negative mass balance since 2000, with mass loss peaking in 2012 and reducing thereafter,  
657 the input-output method data show that the ice sheet was close to a state of balance prior to this  
658 period<sup>40</sup>.

### 659 [Aggregate estimate of ice sheet mass balance](#)

660 To produce an aggregate estimate of Greenland Ice Sheet mass balance, we combine the 14  
661 gravimetry, 9 altimetry, and 3 input-output method datasets to produce a single 26-year record  
662 spanning the period 1992 to 2018. First, we combine the gravimetry, altimetry, and the input-output  
663 method data separately into three time-series by forming an error-weighted average of individual  
664 rates of ice sheet mass change computed using the same technique (Extended Data Figure 6). At  
665 each epoch, we estimate the uncertainty of these time-series as the root mean square of their  
666 component time-series errors. We then combine the mass balance time-series derived from  
667 gravimetry, altimetry, and the input-output method to produce a single, aggregate (reconciled)  
668 estimate, computed as the error-weighted mean of mass trends sampled at each epoch. We  
669 estimated the uncertainty of this reconciled rate of mass balance as either the root mean square

670 departure of the constituent mass trends from their weighted-mean or the root mean square of  
671 their uncertainties, whichever is larger, divided by the square root of the number of independent  
672 satellite techniques used to form the aggregate. Cumulative uncertainties are computed as the root  
673 sum square of annual errors, on the assumption that annual errors are not correlated over time. This  
674 assumption has been employed in numerous mass balance studies<sup>1,18,40,51</sup>, and its effect is to reduce  
675 cumulative errors by a factor 2.2 over the 5-year periods we employ in this study (Table 1). If some  
676 sources of error are temporally correlated, the cumulative uncertainty may therefore be  
677 underestimated. In a recent study, for example, it is estimated that 30 % of the annual mass balance  
678 error is systematic (Shepherd et al., 2019), and in this instance the cumulative error may be 37 %  
679 larger. On the other hand, the estimated annual error on aggregate mass trends reported in this  
680 study (61 Gt/yr) are 70% larger than the spread of the independent estimates from which they are  
681 combined (36 Gt/yr)(Extended Data Table 3), which suggests the underlying errors may be  
682 overestimated by a similar degree. A more detailed analysis of the measurement and systematic  
683 errors is required to improve the cumulative error budget.

684 During the period 2004 to 2015, when all three satellite techniques were in operation, there is good  
685 agreement between changes in ice sheet mass balance on a variety of timescales (Extended Data  
686 Figure 6). In Greenland, there are large annual cycles in mass superimposed on equally prominent  
687 interannual fluctuations as well as variations of intermediate (~5 years) duration. These signals are  
688 consistent with fluctuations in SMB that have been identified in meteorological records<sup>1,80</sup>, and are  
689 present within the time-series of mass balance emerging from all three satellite techniques, to  
690 varying degrees, according to their effective temporal resolution. For example, correlated seasonal  
691 cycles are apparent in the gravimetry and input-output method mass balance time series, because  
692 their effective temporal resolutions are sufficiently short (0.08 and 0.14 years, respectively) to  
693 resolve such changes. However, at 0.74 years, the effective temporal resolution of the altimetry  
694 mass balance time series is too coarse to detect cycles on sub-annual timescales. Nevertheless,  
695 when the aggregated mass balance data emerging from all three experiment groups are degraded to  
696 a common temporal resolution of 36 months, the time-series are well correlated ( $0.63 < r^2 < 0.80$ ) and,  
697 over longer periods, all techniques identify the marked increases in Greenland Ice Sheet mass loss  
698 peaking in 2012. During the period 2005 to 2015, annual rates of mass change determined from all  
699 three techniques differ by up to 137 Gt/yr on average, and their average standard deviation is 36 Gt/yr  
700 - a value that is small or compared to their estimated uncertainty (61 Gt/yr)(Extended Data Table -3).

## 701 Data availability

702 The aggregated Greenland Ice Sheet mass-balance data generated in this study are freely available  
703 at <http://www.imbie.org/data-downloads>.

## 704 Extended Data Legends

705 **Extended Data Figure 1** | Ice sheet mass balance data sets used in this study and their main  
706 contributors (top) and the number and class of data available in each calendar year  
707 (bottom). The interval 2003 to 2010 includes almost all datasets and is selected as the  
708 overlap period. Further details of the satellite observations used in this study are provided  
709 in Supplementary Table 1.

710 **Extended Data Figure 2** | Greenland Ice Sheet drainage basins used in this study, according  
711 to the definitions of ref<sup>21</sup> (left) and ref<sup>46</sup> (right).

712 **Extended Data Figure 3** | Bedrock uplift rates in Greenland averaged over the glacial  
713 isostatic adjustment (GIA) model solutions used in this study (left), as well as their standard  
714 deviation (right). Further details of the GIA models used in this study are provided in  
715 Extended Data Table 1. High rates of uplift and subsidence associated with the former  
716 Laurentide Ice Sheet are apparent to the southwest of Greenland.

717 **Extended Data Figure 4** | Time series of surface mass balance (SMB) in Greenland Ice Sheet  
718 drainage basins<sup>81,82</sup>. Solid lines are annual averages of the monthly data (dashed lines).  
719 Further details of the SMB models used in this study are provided in Extended Data Table 2.

720 **Extended Data Figure 5** | Individual rates of Greenland ice-sheet mass balance used in this  
721 study as determined from satellite altimetry (a, left), gravimetry (b, centre) and the input-  
722 output method (c, right). The light-grey shading shows the estimated  $1\sigma$  uncertainty relative  
723 to the ensemble average. The standard error of the mean solutions, per epoch, is shown in  
724 mid-grey.

725 **Extended Data Figure 6** | Rate of Greenland Ice Sheet mass balance as derived from the  
726 three techniques of satellite radar and laser altimetry (red), input-output method (blue),  
727 and gravimetry (green), and their arithmetic mean (gray), with uncertainty ranges (light  
728 shading).

729 **Extended Data Figure 7** | **Cumulative Greenland Ice Sheet surface mass balance.** The  
730 cumulative surface mass change (lightest blue) determined from an average of the  
731 RACMO2.3p2<sup>59</sup> (light blue), MARv3.6<sup>22</sup> (mid-blue) and HIRHAM<sup>9</sup> (dark blue) regional  
732 climate models relative to their 1980-1990 means (see Methods). The estimated uncertainty  
733 of the average change is also shown (shaded area) is computed as the average of the  
734 uncertainties from each of the three models. RACMO2.3p2 uncertainties are based upon a  
735 comparison to in-situ observations<sup>40</sup>. MARv3.6 uncertainties are evaluated from the  
736 variability due to forcing from climate reanalyses<sup>22</sup>. HIRHAM uncertainties are estimated  
737 based on comparisons to in-situ accumulation and ablation data<sup>83</sup>. Cumulative uncertainties  
738 are computed as the root sum square of annual errors, on the assumption that these errors  
739 are not correlated over time<sup>18</sup>.

740 **Extended Data Table 1.** Details of Glacial Isostatic Adjustment (GIA) models used in this  
741 study.

742 †Regional changes in mass associated with the GIA signal determined by the contributor.

743 ‡Regional changes in mass associated with the GIA signal calculated as an indicative rate  
744 using spherical-harmonic degrees 3 to 90 and a common treatment of degree 2<sup>88</sup>.

745 <sup>a</sup> Main reference publication(s).

746 <sup>b</sup> Model from main publication unless otherwise stated. Comma-separated values refer to  
747 properties of a radially varying (1D, one-dimensional) Earth model: the first value is  
748 lithosphere thickness (km), other values reflect mantle viscosity ( $\times 10^{21}$  Pa s) for specific  
749 layers; see relevant publication.

750 <sup>c</sup> GIA model details: SH=spherical harmonic (maximum degree indicated), FE=finite element,  
751 C=compressible, IC=incompressible, RF=rotational feedback, SG=self-gravitation, OL=ocean  
752 loading, 'x' = feature not included.

753 <sup>d</sup> RSL = relative sea-level data; GPS rates corrected for elastic response to contemporary ice  
754 mass change.

755 <sup>e</sup> Earth model taken from ref<sup>53</sup>

756 <sup>f</sup> Ice model taken from ref<sup>53</sup>

757 <sup>g</sup> Different to ICE-6G\_C in Antarctica, owing to the use of BEDMAP2<sup>89</sup> topography.

758 **Extended Data Table 2.** Details of the surface mass balance (SMB) models used in this study.

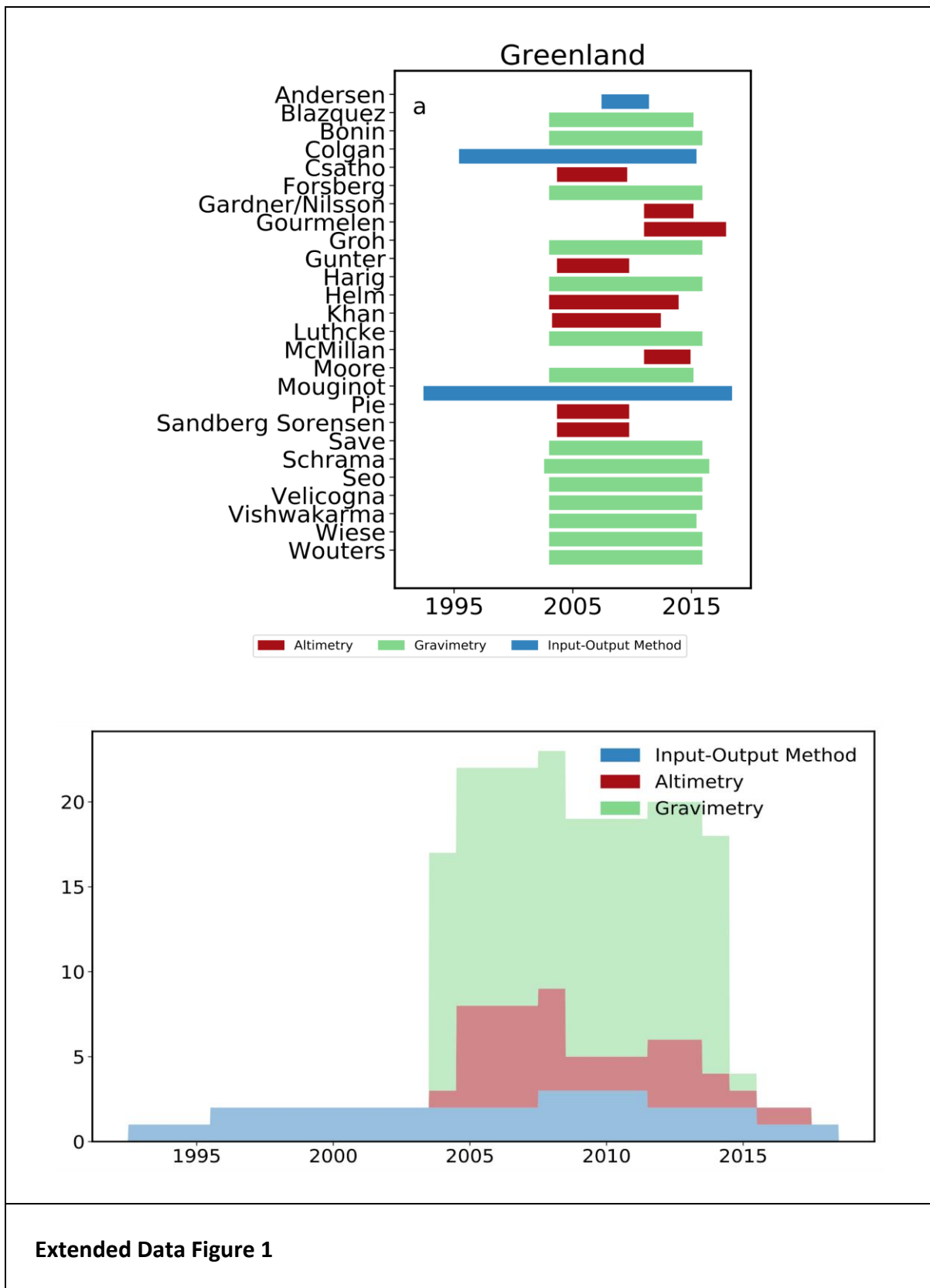
759 <sup>a</sup> Main reference publication; additional references are provided in Supplementary Table 1.

760 <sup>b</sup> SMB model class; regional climate model (RCM), global numerical analysis (GA), process  
761 model (PM). Native resolution (n) and downscaled (d) models are also identified.

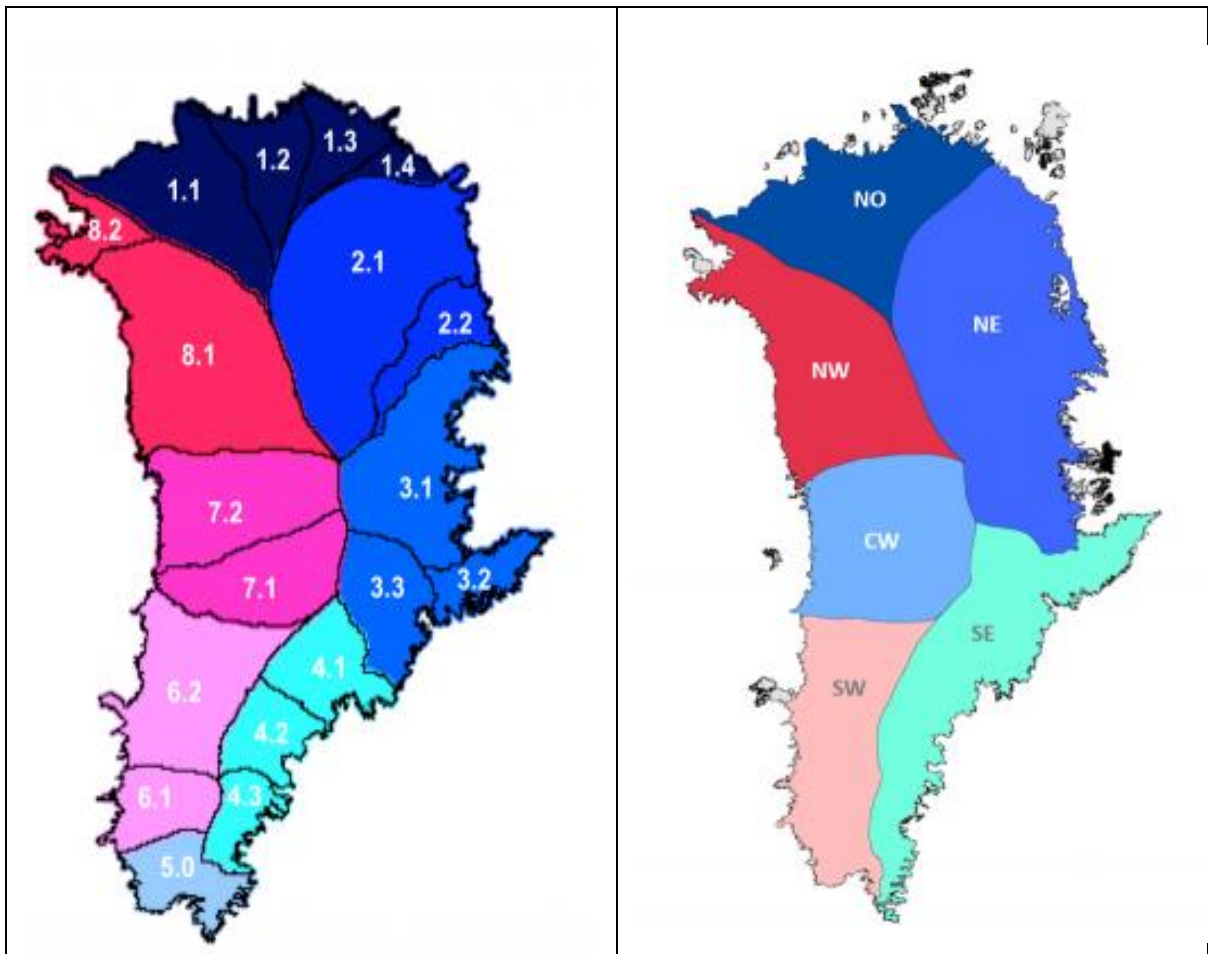
762 <sup>c</sup> Averages over the period 1980 to 2012 for the Greenland Ice Sheet excluding peripheral  
763 ice caps and using the drainage basins from ref<sup>46</sup>.

764 **Extended Data Table 3:** Estimates of ice-sheet mass balance from satellite altimetry,  
765 gravimetry the input–output method, and from all three groups during the period 2005 to  
766 2015. Also shown are the average standard deviations (s.d.) and ranges of individual  
767 estimates within each group during the same period.

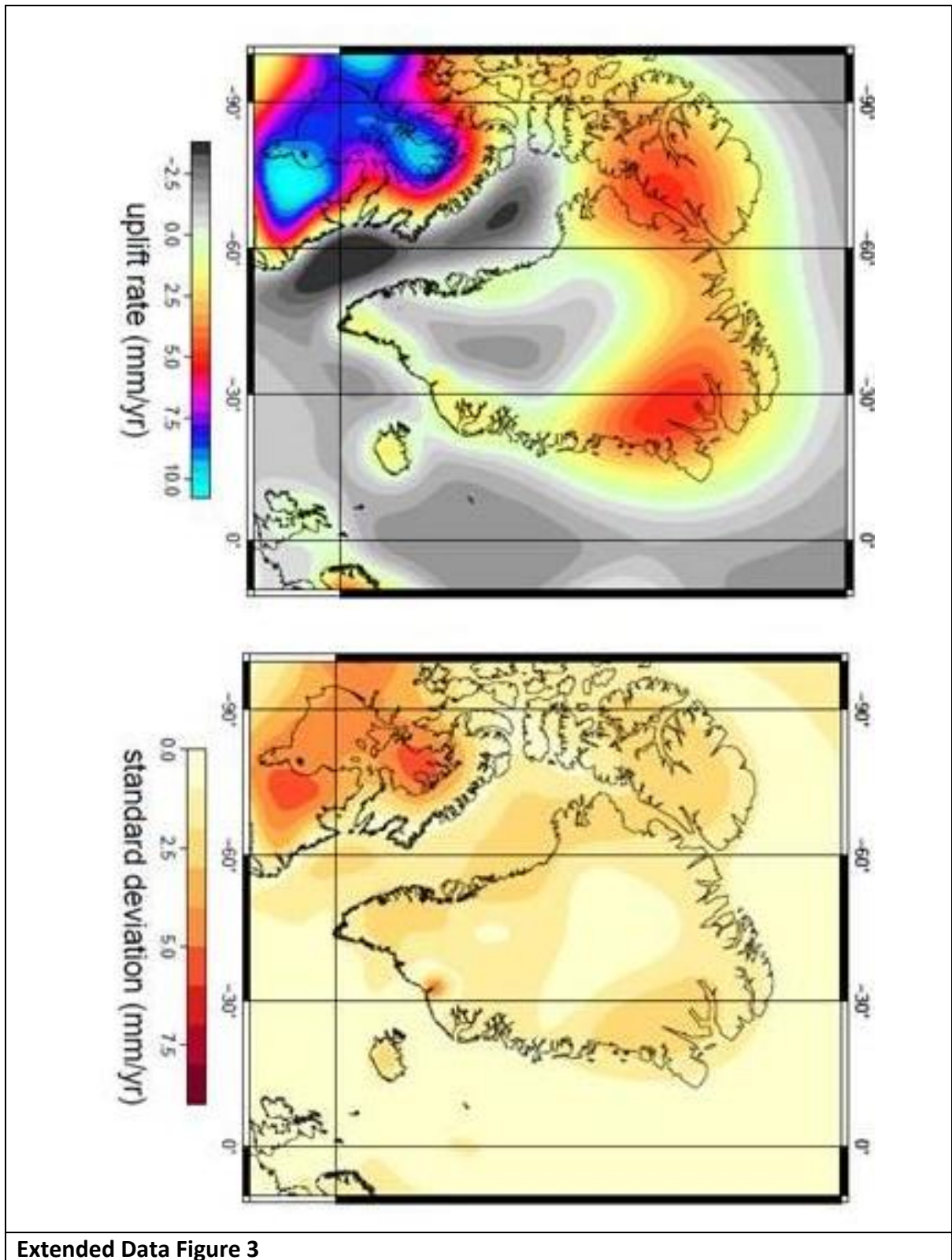
768 \*No altimetry data in 2010.



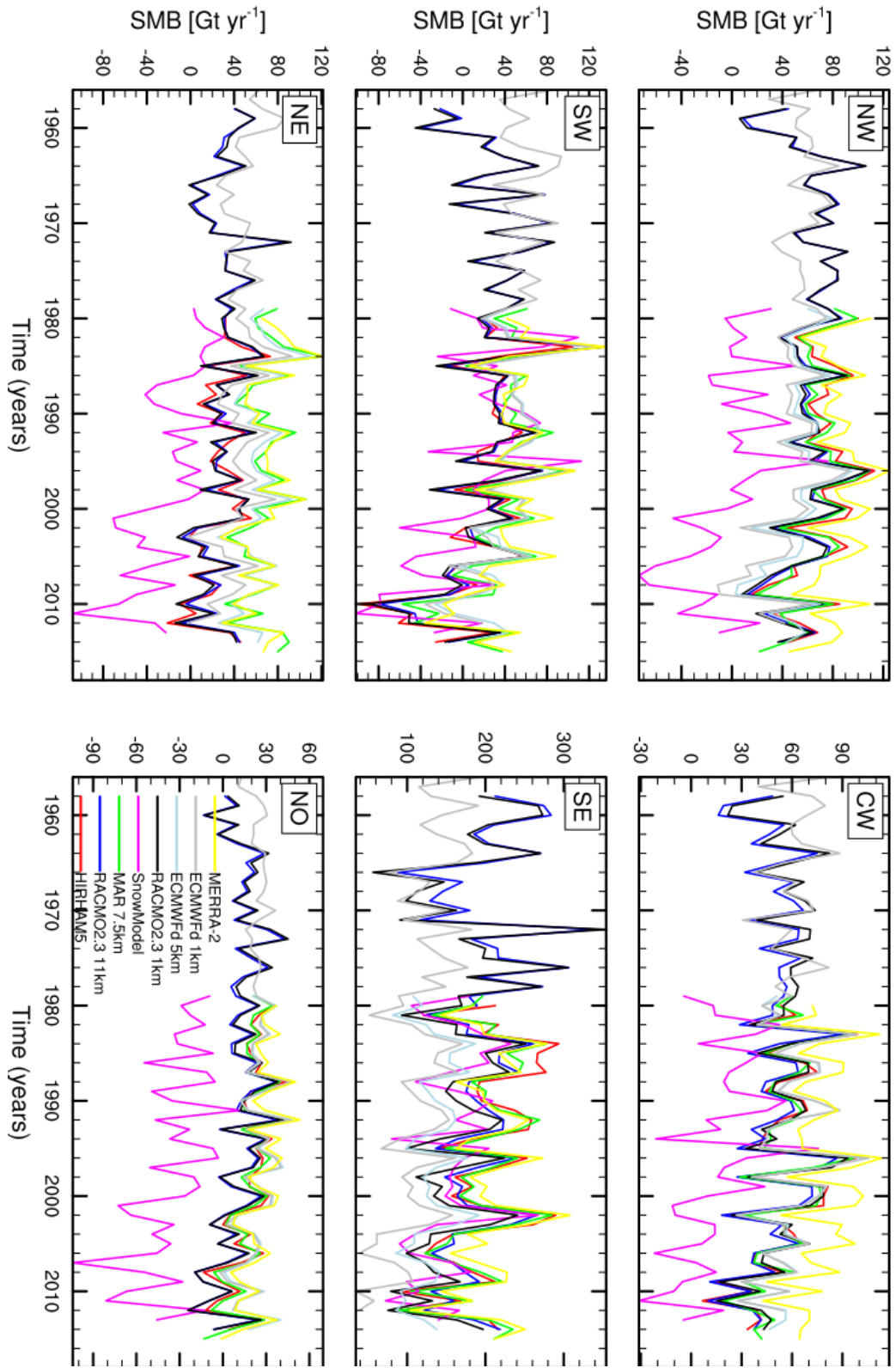
Extended Data Figure 1



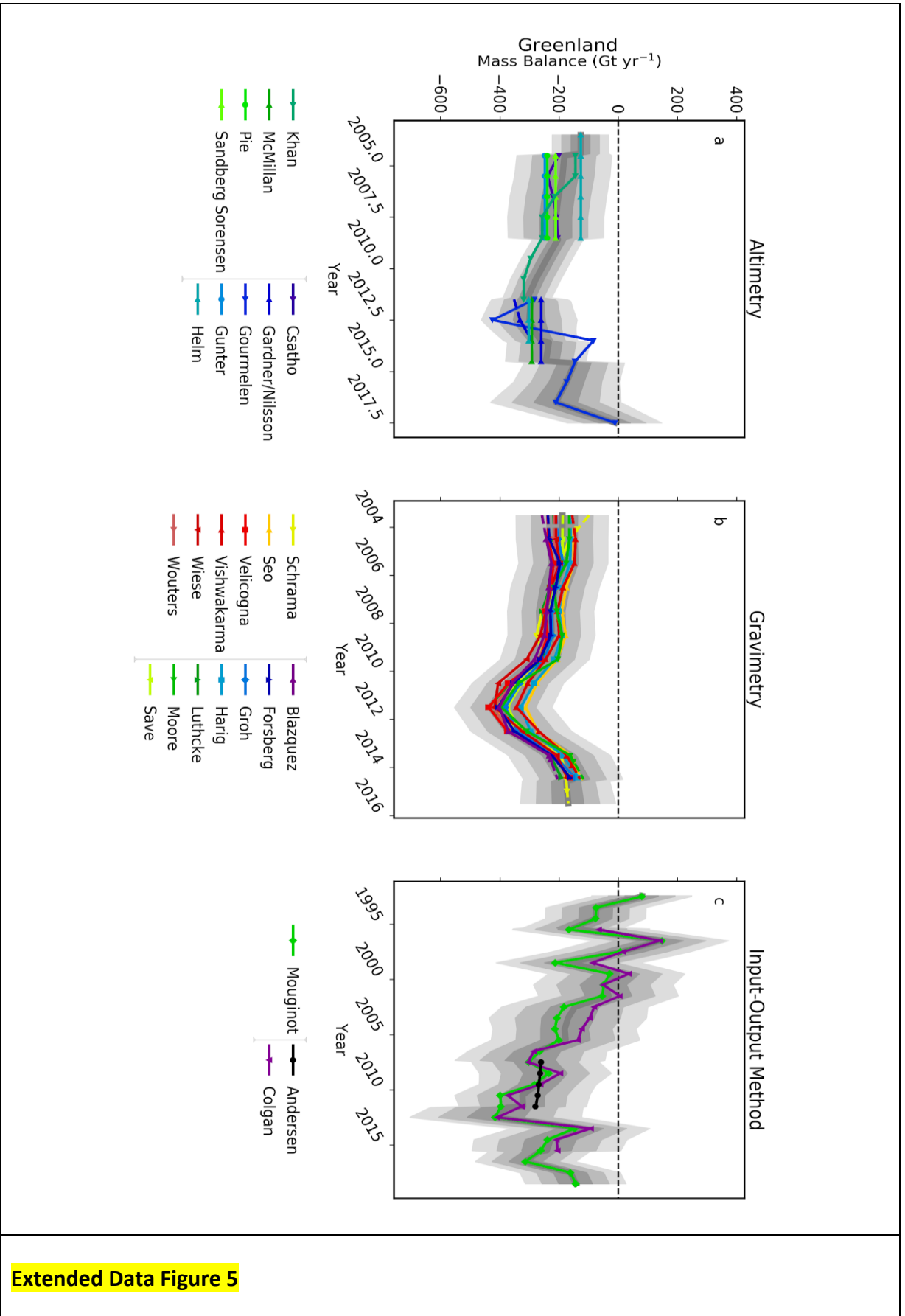
Extended Data Figure 2



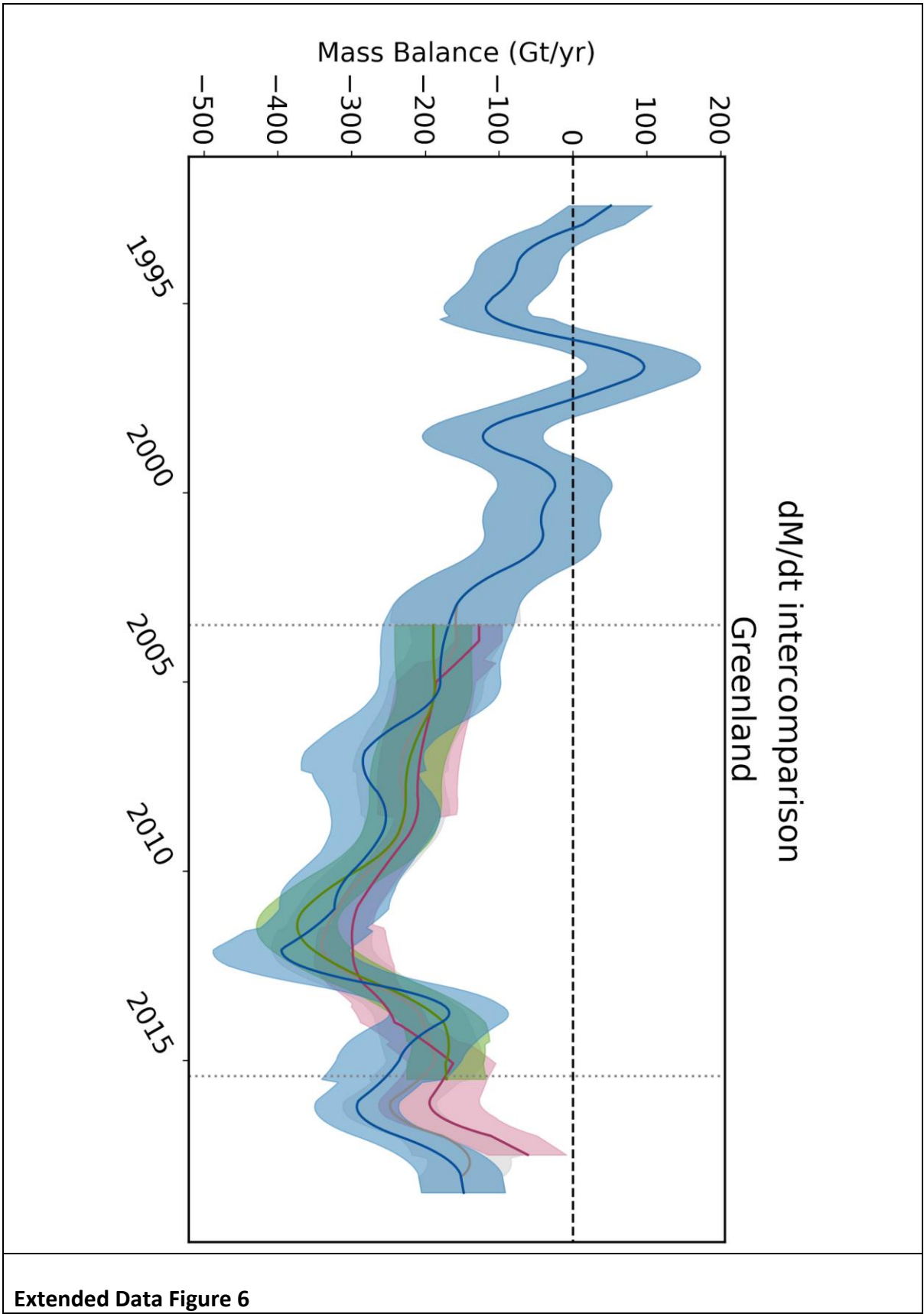
Extended Data Figure 3



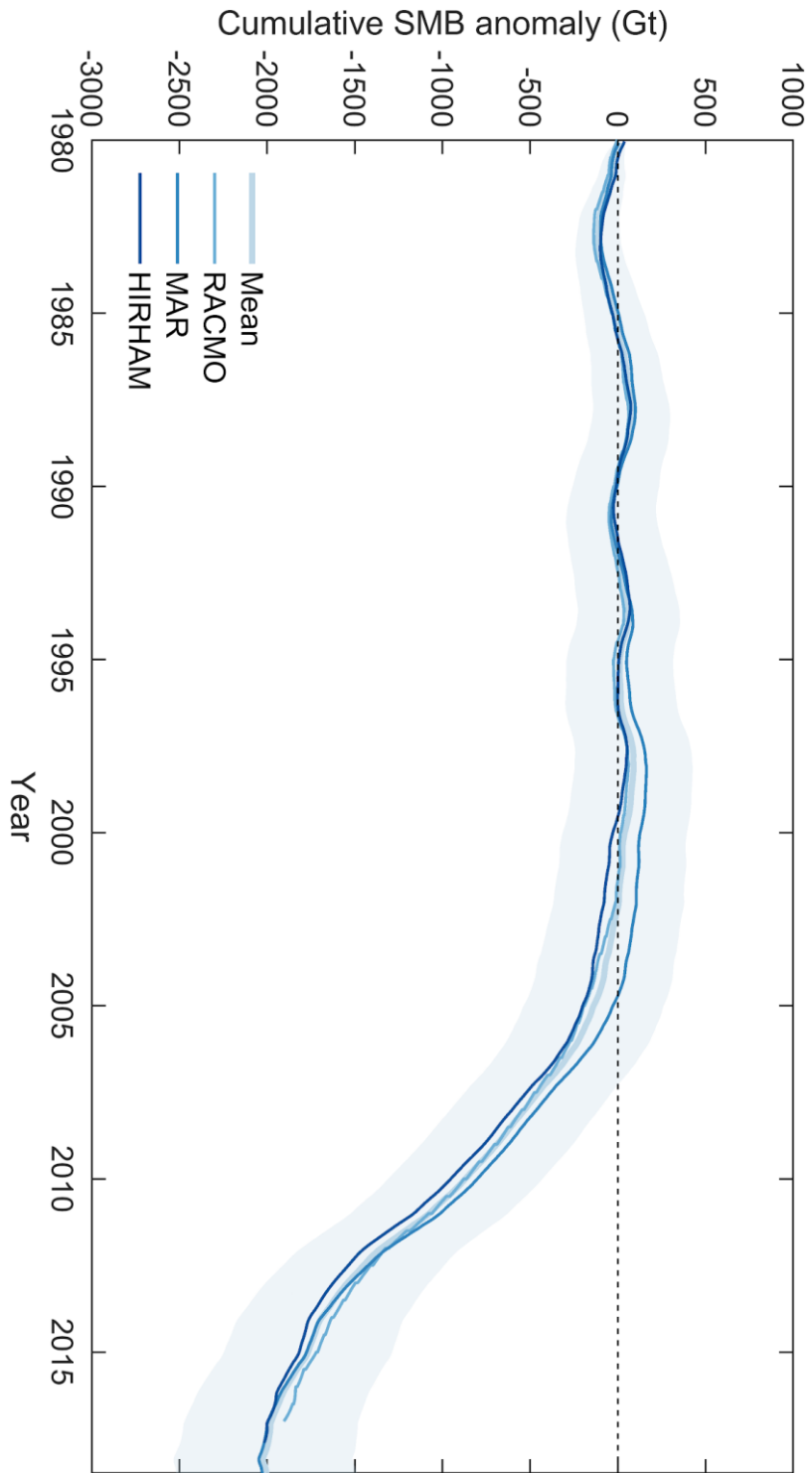
Extended Data Figure 4



**Extended Data Figure 5**



Extended Data Figure 6



Extended Data Figure 7

Contributor	Model	Publication <sup>a</sup>	Earth model <sup>b</sup>	Ice model <sup>b</sup>	GIA model <sup>c</sup>	Constraint data <sup>d</sup>	GIA (Gt/yr)
A	A13	<sup>76</sup>	VM5a (1D) <sup>e</sup>	ICE-6G_C <sup>f</sup>	SH, C, RF, SG, OL	As for ICE-6G_C <sup>f</sup>	-9 <sup>‡</sup>
Lecavalier	Huy3	<sup>41</sup>	1D (120, 0.5, 2)	Huy3/ICE-5G	SH(256), IC, RF, SG, OL	RSL, ice extent, paleo thinning rates	-19 <sup>‡</sup>
Sasgen	GGG1D.0	<sup>52,84</sup>	VM-GPS <sup>52</sup>	modified GREEN1 <sup>85</sup>	SH(256)/FE(radial), IC, RF, SG, OL	GPS, RSL	+17 <sup>‡</sup>
Peltier	ICE-6G_D (VM5a)	<sup>53</sup>	VM5a (1D) <sup>e</sup>	ICE-6G_D <sup>g</sup>	SH(512)	GPS, RSL, Earth rotation	-10 <sup>‡</sup>
van der Wal	SL-dry-4mm/W12	<sup>86</sup>	3D, power-law rheology	Combination of W12 (Antarctica) and ICE-5G	FE, IC, xRF	GPS, RSL, seismic velocities (Earth model)	+21 <sup>‡</sup>
Spada	SELEN 4	<sup>87</sup>	VM5a (3-layer average of 1D model) <sup>e</sup>	ICE-6G_C <sup>f</sup>	SELEN4: SH(128), IC, RF, SG, OL	As for ICE-6G_C <sup>f</sup>	-27 <sup>‡</sup>
<b>Extended Data Table 1</b>							

Contributor	Model	Publication <sup>a</sup>	Class <sup>b</sup>	Area (10 <sup>6</sup> km <sup>2</sup> )	Grid	SMB <sup>c</sup> (Gt/yr)	Precipitation <sup>c</sup> (Gt/yr)	Runoff <sup>c</sup> (Gt/yr)
Noël	RACMO2.3	<sup>90</sup>	RCM	1.73	11 km	350	721	311
Noël	RACMO2.3p2	<sup>59</sup>	RCM	1.73	11 km	432	727	258
Langen	HIRHAM5	<sup>9</sup>	RCM	1.71	5.5 km	385	794	351
Fettweis	MARv3.6	<sup>22</sup>	RCM	1.69	7.5 km	381	706	308
Noël	RACMO2.3d	<sup>91</sup>	RCM-d	1.69	1 km	314	755	397
Noël	RACMO2.3p2d	<sup>59</sup>	RCM-d	1.69	1 km	338	703	331
Cullather	MERRA-2	<sup>92</sup>	GA-n	1.73	0.5 °	504	818	277
Hanna	ECMWF	<sup>14</sup>	GA-d	1.65	5 km	370	532	186
Wilton	ECMWFd	<sup>93</sup>	GA-d	1.71	1 km	314	603	246
Mernild	Snow Model	<sup>94</sup>	PM	1.64	5 km	125	655	418
<b>Extended Data Table 2</b>								

786

Technique	Mass balance (Grt/yr)	s.d.(Gt/yr)	range (Gt/yr)
Altimetry*	-237 ± 46	31	84
Gravimetry	-250 ± 52	26	86
Input-Output Method	-269 ± 80	22	47
All	-249 ± 61	36	137

**Extended Data Table 3**

787

788 [Supplementary Information](#)

This table is an excel spreadsheet

**Supplementary Table 1** This table contains details of the satellite datasets used in this study <sup>35,36,40,73,77,80,95-118</sup>.

789

## 790 Additional References

791

- 792 72 Wahr, J., Wingham, D. & Bentley, C. A method of combining ICESat and GRACE satellite data  
793 to constrain Antarctic mass balance. *Journal of Geophysical Research-Solid Earth* **105**, 16279-  
794 16294 (2000).
- 795 73 Paulson, A., Zhong, S. & Wahr, J. Inference of mantle viscosity from GRACE and relative sea  
796 level data. *Geophysical Journal International* **171**, 497-508, doi:10.1111/j.1365-  
797 246X.2007.03556.x (2007).
- 798 74 Peltier, W. R. in *Annual Review of Earth and Planetary Sciences* Vol. 32 111-149 (2004).
- 799 75 Simpson, M. J. R., Milne, G. A., Huybrechts, P. & Long, A. J. Calibrating a glaciological model  
800 of the Greenland ice sheet from the Last Glacial Maximum to present-day using field  
801 observations of relative sea level and ice extent. *Quaternary Science Reviews* **28**, 1631-1657,  
802 doi:10.1016/j.quascirev.2009.03.004 (2009).
- 803 76 A, G., Wahr, J. & Zhong, S. Computations of the viscoelastic response of a 3-D compressible  
804 earth to surface loading: An application to glacial isostatic adjustment in Antarctica and  
805 Canada. *Geophysical Journal International* **192**, 557-572, doi:10.1093/gji/ggs030 (2013).
- 806 77 Schrama, E. J. O., Wouters, B. & Rietbroek, R. A mascon approach to assess ice sheet and  
807 glacier mass balances and their uncertainties from GRACE data. *J. Geophys. Res. B Solid Earth*  
808 **119**, 6048-6066, doi:10.1002/2013JB010923 (2014).
- 809 78 Klemann, V. & Martinec, Z. Contribution of glacial-isostatic adjustment to the geocenter  
810 motion. *Tectonophysics* **511**, 99-108, doi:10.1016/j.tecto.2009.08.031 (2011).
- 811 79 Rignot, E. *et al.* Recent Antarctic ice mass loss from radar interferometry and regional  
812 climate modelling. *Nature Geoscience* **1**, 106-110, doi:10.1038/ngeo102 (2008).
- 813 80 Wouters, B., Bamber, J. L., Van Den Broeke, M. R., Lenaerts, J. T. M. & Sasgen, I. Limits in  
814 detecting acceleration of ice sheet mass loss due to climate variability. *Nature Geoscience* **6**,  
815 613-616, doi:10.1038/ngeo1874 (2013).
- 816 81 Rignot, E., Mouginot, J. & Scheuchl, B. Ice Flow of the Antarctic Ice Sheet. *Science* **333**, 1427-  
817 1430, doi:10.1126/science.1208336 (2011).
- 818 82 Rignot, E., Mouginot, J. & Scheuchl, B. Antarctic grounding line mapping from differential  
819 satellite radar interferometry. *Geophysical Research Letters* **38**, doi:10.1029/2011GL047109  
820 (2011).
- 821 83 Langen, P. L., Fausto, R. S., Vandecrux, B., Mottram, R. H. & Box, J. E. Liquid water flow and  
822 retention on the Greenland ice sheet in the regional climate model HIRHAM5: Local and  
823 large-scale impacts. *Front. Earth Sci.* **4**, doi:10.3389/feart.2016.00110 (2017).
- 824 84 Martinec, Z. Spectral-finite element approach to three-dimensional viscoelastic relaxation in  
825 a spherical earth. *Geophysical Journal International* **142**, 117-141, doi:10.1046/j.1365-  
826 246X.2000.00138.x (2000).
- 827 85 Fleming, K. & Lambeck, K. Constraints on the Greenland Ice Sheet since the Last Glacial  
828 Maximum from sea-level observations and glacial-rebound models. *Quaternary Science*  
829 *Reviews* **23**, 1053-1077, doi:10.1016/j.quascirev.2003.11.001 (2004).
- 830 86 King, M. A., Whitehouse, P. L. & van der Wal, W. Incomplete separability of Antarctic plate  
831 rotation from glacial isostatic adjustment deformation within geodetic observations.  
832 *Geophysical Journal International* **204**, 324-330, doi:10.1093/gji/ggv461 (2016).
- 833 87 SELEN v2.9.13 [software] (2018).
- 834 88 Martinec, Z. & Hagedoorn, J. The rotational feedback on linear-momentum balance in glacial  
835 isostatic adjustment. *Geophysical Journal International* **199**, 1823-1846,  
836 doi:10.1093/gji/ggu369 (2014).
- 837 89 Fretwell, P. *et al.* Bedmap2: Improved ice bed, surface and thickness datasets for Antarctica.  
838 *Cryosphere* **7**, 375-393, doi:10.5194/tc-7-375-2013 (2013).

839 90 Noël, B. *et al.* Evaluation of the updated regional climate model RACMO2.3: Summer  
840 snowfall impact on the Greenland Ice Sheet. *Cryosphere* **9**, 1831-1844, doi:10.5194/tc-9-  
841 1831-2015 (2015).

842 91 Noël, B. *et al.* A daily, 1 km resolution data set of downscaled Greenland ice sheet surface  
843 mass balance (1958-2015). *Cryosphere* **10**, 2361-2377, doi:10.5194/tc-10-2361-2016 (2016).

844 92 Gelaro, R. *et al.* The modern-era retrospective analysis for research and applications, version  
845 2 (MERRA-2). *Journal of Climate* **30**, 5419-5454, doi:10.1175/JCLI-D-16-0758.1 (2017).

846 93 Wilton, D. J. *et al.* High resolution (1 km) positive degree-day modelling of Greenland ice  
847 sheet surface mass balance, 1870-2012 using reanalysis data. *Journal of Glaciology* **63**, 176-  
848 193, doi:10.1017/jog.2016.133 (2017).

849 94 Mernild, S. H., Liston, G. E., Hiemstra, C. A. & Christensen, J. H. Greenland Ice Sheet Surface  
850 Mass-Balance Modeling in a 131-Yr Perspective, 1950-2080. *Journal of Hydrometeorology*  
851 **11**, 3-25 (2010).

852 95 Bonin, J. & Chambers, D. Uncertainty estimates of a GRACE inversion modelling technique  
853 over greenland using a simulation. *Geophysical Journal International* **194**, 212-229,  
854 doi:10.1093/gji/ggt091 (2013).

855 96 Blazquez, A. *et al.* Exploring the uncertainty in GRACE estimates of the mass redistributions  
856 at the Earth surface: Implications for the global water and sea level budgets. *Geophysical*  
857 *Journal International* **215**, 415-430, doi:10.1093/gji/ggy293 (2018).

858 97 Forsberg, R., Sørensen, L. & Simonsen, S. Greenland and Antarctica Ice Sheet Mass Changes  
859 and Effects on Global Sea Level. *Surveys in Geophysics* **38**, 89-104, doi:10.1007/s10712-016-  
860 9398-7 (2017).

861 98 Groh, A. & Horwath, M. in *European Geophysical Union* (Vienna, 2016).

862 99 Harig, C. & Simons, F. J. Mapping Greenland's mass loss in space and time. *Proceedings of*  
863 *the National Academy of Sciences of the United States of America* **109**, 19934-19937,  
864 doi:10.1073/pnas.1206785109 (2012).

865 100 Luthcke, S. B. *et al.* Antarctica, Greenland and Gulf of Alaska land-ice evolution from an  
866 iterated GRACE global mascon solution. *Journal of Glaciology* **59**, 613-631,  
867 doi:10.3189/2013JoG12J147 (2013).

868 101 Andrews, S. B., Moore, P. & King, M. A. Mass change from GRACE: A simulated comparison  
869 of Level-1B analysis techniques. *Geophysical Journal International* **200**, 503-518,  
870 doi:10.1093/gji/ggu402 (2015).

871 102 Save, H., Bettadpur, S. & Tapley, B. D. High-resolution CSR GRACE RL05 mascons. *J. Geophys.*  
872 *Res. B Solid Earth* **121**, 7547-7569, doi:10.1002/2016JB013007 (2016).

873 103 Seo, K. W. *et al.* Surface mass balance contributions to acceleration of Antarctic ice mass loss  
874 during 2003-2013. *J. Geophys. Res. B Solid Earth* **120**, 3617-3627, doi:10.1002/2014JB011755  
875 (2015).

876 104 Velicogna, I., Sutterley, T. C. & Van Den Broeke, M. R. Regional acceleration in ice mass loss  
877 from Greenland and Antarctica using GRACE time-variable gravity data. *Geophysical*  
878 *Research Letters* **41**, 8130-8137, doi:10.1002/2014GL061052 (2014).

879 105 Vishwakarma, B. D., Horwath, M., Devaraju, B., Groh, A. & Sneeuw, N. A Data-Driven  
880 Approach for Repairing the Hydrological Catchment Signal Damage Due to Filtering of GRACE  
881 Products. *Water Resources Research* **53**, 9824-9844, doi:10.1002/2017WR021150 (2017).

882 106 Wiese, D. N., Landerer, F. W. & Watkins, M. M. Quantifying and reducing leakage errors in  
883 the JPL RL05M GRACE mascon solution. *Water Resources Research* **52**, 7490-7502,  
884 doi:10.1002/2016WR019344 (2016).

885 107 Cheng, M., Tapley, B. D. & Ries, J. C. Deceleration in the Earth's oblateness. *J. Geophys. Res.*  
886 *B Solid Earth* **118**, 740-747, doi:10.1002/jgrb.50058 (2013).

887 108 Swenson, S., Chambers, D. & Wahr, J. Estimating geocenter variations from a combination of  
888 GRACE and ocean model output. *J. Geophys. Res. B Solid Earth* **113**,  
889 doi:10.1029/2007JB005338 (2008).

890 109 Csatho, B. M. *et al.* Laser altimetry reveals complex pattern of Greenland Ice Sheet  
891 dynamics. *Proceedings of the National Academy of Sciences of the United States of America*  
892 **111**, 18478-18483, doi:10.1073/pnas.1411680112 (2014).

893 110 Nilsson, J., Gardner, A., Sørensen, L. S. & Forsberg, R. Improved retrieval of land ice  
894 topography from CryoSat-2 data and its impact for volume-change estimation of the  
895 Greenland Ice Sheet. *Cryosphere* **10**, 2953-2969, doi:10.5194/tc-10-2953-2016 (2016).

896 111 Gourmelen, N. *et al.* CryoSat-2 swath interferometric altimetry for mapping ice elevation  
897 and elevation change. *Advances in Space Research* **62**, 1226-1242,  
898 doi:10.1016/j.asr.2017.11.014 (2018).

899 112 Gunter, B. C. *et al.* Empirical estimation of present-day Antarctic glacial isostatic adjustment  
900 and ice mass change. *Cryosphere* **8**, 743-760, doi:10.5194/tc-8-743-2014 (2014).

901 113 Felikson, D. *et al.* Comparison of Elevation Change Detection Methods from ICESat Altimetry  
902 over the Greenland Ice Sheet. *IEEE Transactions on Geoscience and Remote Sensing* **55**,  
903 5494-5505, doi:10.1109/TGRS.2017.2709303 (2017).

904 114 Helm, V., Humbert, A. & Miller, H. Elevation and elevation change of Greenland and  
905 Antarctica derived from CryoSat-2. *Cryosphere* **8**, 1539-1559, doi:10.5194/tc-8-1539-2014  
906 (2014).

907 115 Kjeldsen, K. K. *et al.* Improved ice loss estimate of the northwestern Greenland ice sheet. *J.*  
908 *Geophys. Res. B Solid Earth* **118**, 698-708, doi:10.1029/2012JB009684 (2013).

909 116 Khan, S. A. *et al.* Sustained mass loss of the northeast Greenland ice sheet triggered by  
910 regional warming. *Nat. Clim. Change* **4**, 292-299, doi:10.1038/nclimate2161 (2014).

911 117 Andersen, M. L. *et al.* Basin-scale partitioning of Greenland ice sheet mass balance  
912 components (2007-2011). *Earth and Planetary Science Letters* **409**, 89-95,  
913 doi:10.1016/j.epsl.2014.10.015 (2015).

914 118 Colgan, W. *et al.* Greenland ice sheet mass balance assessed by PROMICE (1995–2015).  
915 *GEUS Bulletin* **43** (2019).

916